R. & M. No. 2680
(10,709)
A.R.C. Technical Report

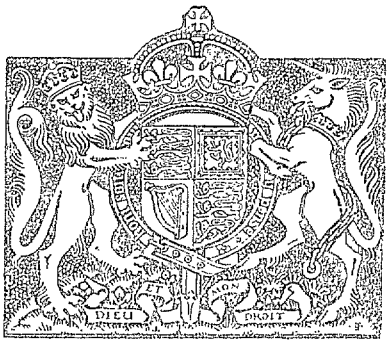

MINISTRY OF SUPPLY

AERONAUTICAL RESEARCH COUNCIL
REPORTS AND MEMORANDA

Measurements of Mid-chord Pitching Moment Derivatives at High Speeds

By

J. B. BRATT, B.A., B.Sc., and A. CHINNECK,
of the Aerodynamics Division, N.P.L.

LONDON : HER MAJESTY'S STATIONERY OFFICE
1954
PRICE 9s 6d NET

Measurements of Mid-chord Pitching Moment Derivatives at High Speeds

By

J. B. BRATT, B.A., B.Sc., and A. CHINNECK,
of the Aerodynamics Division, N.P.L.

Reports and Memoranda No. 2680*

June, 1947

Summary.—Measurements of the pitching moment derivative coefficients $m_{\dot{\alpha}}$ and m_{α} for a $7\frac{1}{2}$ per cent bi-convex aerofoil oscillating about the mid-chord axis were made in a high-speed wind tunnel by the method of decaying oscillations. The tests were made at Mach numbers of 1·275, 1·455 and 1·515 for supersonic flow, and covered a range extending from 0·4 to 0·9 at subsonic speeds. The effect of variation of frequency parameter was also investigated, and conditions giving rise to sustained or growing oscillations at subsonic speeds were examined.

Comparison with existing flat plate theories for supersonic flow shows complete disagreement in the trend of the damping with Mach number change, the linearized theory for a flat plate giving an increasing negative value as M is reduced below 1·41, whereas experiment gives an increasing positive value. A recent theory which takes into account the shape of the profile agrees in trend with experiment, suggesting that profile is of vital importance in this field.

The results of the subsonic tests exhibit a narrow region of Mach number extending from approximately 0·87 to 0·89 within which negative damping can arise. It is thought that this effect is bound up with the formation of shock-waves at the surface of the model.

1. *Introduction.*—The work described in this paper was carried out in the 1-ft Circular High-Speed Tunnel at the National Physical Laboratory, and measurements of the damping and stiffness derivative coefficients for a $7\frac{1}{2}$ per cent bi-convex aerofoil of 2-in. chord, oscillating about the half-chord axis in two-dimensional flow, were obtained at both supersonic and subsonic speeds. In the first instance, the tests were planned to check the theoretical prediction of negative damping for pitching oscillations about the half-chord axis in supersonic flow at low values of the frequency parameter $(2\pi fc/V)$ and values of Mach number below $M = \sqrt{2}$. Advantage was taken of the fact that the tunnel could be run at subsonic speeds, and a series of measurements was also obtained for Mach numbers ranging up to approximately $M = 0{\cdot}9$. The production of sustained or growing oscillations at subsonic speeds was also investigated.

The method of decaying or growing oscillations was employed, since this offered a straightforward means of measuring damping, which did not require the development of complicated apparatus. It was found possible, however, to determine also the aerodynamic stiffness from an accurate measurement of the change in natural frequency of the system due to the air forces.

A further object of these experiments was to gain some preliminary experience in the measurement of oscillatory aerodynamic forces at high speeds with a view to designing equipment for measuring a complete set of two-dimensional derivative coefficients relating to flexure-torsion flutter.

* Published with the permission of the Director, National Physical Laboratory.

2. *Description of Apparatus.*—2.1. *General Layout.*—The general arrangement of the apparatus is shown in elevation and in plan form in Figs. 1 and 2 respectively, and photographs of the tunnel working-section are given in Figs. 3 and 4. The tunnel is of the injector type with a working-section in the form of a vertical steel cylinder of 1-ft internal diameter, and the oscillating system was mounted on two horizontal steel platforms P (Fig. 1) attached to opposite sides of the working-section. A solid steel bi-convex aerofoil of 2-in. chord (standard for the tunnel) and $7\frac{1}{2}$ per cent thickness/chord ratio was used for the tests, the bi-convex section being chosen in preference to a double-wedge on account of the greater flexural stiffness for a given thickness/chord ratio.

The model spanned the working-section of the tunnel, and its ends, which passed through clearance holes in the tunnel walls, were clamped to steel cylinders which formed the rotating members of two crossed-spring bearings B, the function of which was to take up the lift and drag on the model whilst allowing freedom to pitch about the half-chord axis. An elastic constraint for pitching displacements was provided by two steel torsion rods R fixed in the bearing cylinders and clamped at their outer ends to earthed brackets (*see* also Fig. 5). In an attempt to increase the effective flexural stiffness of the model the oscillatory system was put under tension, and to allow this the housings of the crossed-spring bearings were floated on vertical spring strips which permitted freedom for axial displacement. The advantage gained by tensioning, however, was not very great, the flexural frequency increasing from 99·0 c.p.s. to 123·3 c.p.s. at the working tension of 1000 lb.

Changes in the natural pitching frequency of the system could be made by attaching masses (shown dotted in Fig. 2) to a horizontal steel arm A fixed to one of the bearing cylinders, the frequency range covered being roughly 8 to 16 c.p.s. Measurements for a torsional mode of oscillation could also be made by rigidly locking the bearing at the end remote from A by means of a special steel clamp. With this arrangement the elastic constraint was provided by the twisting of the aerofoil and one torsion rod and gave a somewhat higher frequency range of approximately 13 to 27 c.p.s.

Since the operation of this type of tunnel leads to a reduced pressure in the working-section (approximately $\frac{1}{3}$ atmospheric at $M = 1{\cdot}4$) it was necessary to box-in the two platforms as indicated by the dotted lines in Fig. 1 in order to prevent flow through the holes in the tunnel walls. The boxes were constructed of steel, with removable sides to allow adjustments to be made.

2.2. *Recording Mechanism.*—For the purpose of recording the motion of the model a light aluminium vane T was fixed to one end of the arm A (Figs. 2, 7) and projected through a slot in the wall of the surrounding box into a small side-box S (*see* also Fig. 6). Immediately behind the vane in the side-box a vertical screen was situated, which carried a patch of white paper glued in such a position as to be half covered by the vane when the model was in its mean position. The patch was shaped as indicated in Fig. 7, and its outer end was slightly overlapped by a straight-edged mask F fixed in front of the vane and adjustable by rotation about the pivot G. All surfaces excepting the white patch were painted dead black.

A lamp L formed a source of illumination, and the light scattered from the patch fell on a photocell C screened from the direct rays of the lamp by a partition. With this arrangement the illumination of the photocell was a function of the displacement of the model, and by adjustment of the mask F a linear relationship was obtainable.

A 1-megohm resistance R was included in the photocell circuit (Fig. 9), and the voltage developed across it formed the input to a commercial-type cathode-ray oscillograph*. The motion of the spot on the oscillograph screen was photographed on a 35-mm film moving continuously in a direction perpendicular to the displacement of the spot.

* Mullard type E 800.

2.3. *Release Mechanism.*—The model could be deflected by means of a plunger D (Figs. 1, 8), which worked in a sleeve fixed to the top of the steel box enclosing the arm A (Fig. 2). Normally the plunger was held clear of the oscillatory system by a spring, but when depressed it came into contact with A near the end remote from the side-box, the amount of deflection of the model being determined by the setting of an adjustable collar K (Fig. 8) in relation to the top of the sleeve. When fully depressed the plunger was held down by a catch which engaged with K and was kept in position against the pull of a spring by the friction at the point of engagement.

The system was released by pulling out the catch which immediately made contact with an insulated screw H and short-circuited a resistance R_2 connected in the photocell circuit between one end of the resistance R_1 and the common earth (Fig. 9). By this arrangement it was possible to avoid large transient effects in the cathode-ray oscillograph due mainly to the change in mean input voltage on release. These effects resulted from the presence of resistance-capacity coupling elements of large time constant in the amplifier circuits of the oscillograph and gave rise to a bodily drift of the oscillating spot across the screen at right angles to the direction of motion of the film. The resistance R_2 was adjusted so that the voltage drop across it was equal to the decrease in voltage across R_1 due to the initial deflection from the mean position. Thus on release the mean input voltage remained unchanged. An analytical treatment of the transient effect in a simple series resistance-capacity circuit is given in an Appendix.

2.4. *Automatic Brake Mechanism.*—In order to safeguard the apparatus under conditions giving rise to negative damping, electrically operated brakes were fitted adjacent to each of the crossed-spring bearings. The braking action was obtained by means of brake blocks carried on two vertical arms M (Fig. 10) pivoted at their lower ends and pulled towards each other by a helical spring. When the brake operated the blocks gripped a brake drum formed by an extension of the bearing cylinder, but they were normally held clear of the drum by the toggle action of two links N joining the upper ends of the arms and held in position by the attraction of an electromagnet W on an armature attached to the junction of the links. Automatic operation of the brakes was obtained by means of contacts included in the electrical circuit and set to be kicked open by arms forming part of the oscillatory system when the amplitude reached a chosen value. A plunger working in a sleeve fixed to the top of the steel box was arranged over each brake for the purpose of resetting the toggle.

2.5. *Time Marker.*—A time scale which consisted of a series of dots spaced at intervals corresponding to $\frac{1}{50}$ sec was included near the edge of each photographic record for the purpose of measuring frequency. The marker consisted of a spark gap situated near the circumference of the oscillograph screen and connected across the secondary circuit of a car induction coil, the primary of which was energised through a contact operated by a standard 50 cycle electrically maintained tuning fork. In order to prevent interference of the image on the screen by the spark it was found necessary to include a 10,000-ohm suppressor resistance in the high-tension lead close to the spark gap, the opposite side of which was earthed. The high-tension lead was electrically screened.

3. *Stiffness Measurements.*—3.1. *Method.*—Moments were applied to the aerofoil system by means of 6-in. steel arms which could be attached to the bearing cylinders, and at their extremities carried steel points on which scale pans could be hung. On account of the uncertainty in the direct measurement of the distance of a point from the axis of rotation, two arms were fixed at each bearing extending in opposite directions. The distance between the points on a pair of arms could be measured accurately, and from a measurement of the displacement of each point when a load was applied at the opposite end of the aerofoil, the ratio and thus the lengths of the moment arms could be determined.

Angular rotations were derived from measurements of the displacement of a point determined with the aid of a micrometer head carried in a rigid clamp. Contact was indicated by the closing of an electric circuit which included a sensitive galvanometer.

3.2. *Dynamic Stiffness.*—The end of the model carrying the aluminium vane was chosen as reference section, and this is referred to in the following discussion as station 1, the opposite end being station 2. Since the stiffness relating to the reference section would be influenced by twist of the aerofoil during a pitching oscillation, it was necessary to examine this effect.

Let α_1, α_2 be angular displacements and m_1, m_2 moments relating to stations 1 and 2 respectively. Then

$$\left.\begin{aligned} \alpha_1 &= a_{11}m_1 + a_{12}m_2, \\ \alpha_2 &= a_{21}m_1 + a_{22}m_2, \end{aligned}\right\} \quad .. \quad .. \quad .. \quad .. \quad .. \quad .. \quad (1)$$

where a_{11}, a_{12}, etc., are influence coefficients. These were determined experimentally by measurement of α_1 and α_2 with m_1 and m_2 applied separately. In matrix notation, equations (1) may be written

$$\{\alpha\} = [a]\{m\} . \quad .. \quad .. \quad .. \quad .. \quad .. \quad .. \quad .. \quad (2)$$

A similar pair of equations involving stiffnesses may be written

$$\left.\begin{aligned} m_1 &= s_{11}\alpha_1 + s_{12}\alpha_2, \\ m_2 &= s_{21}\alpha_1 + s_{22}\alpha_2, \end{aligned}\right\} \quad .. \quad .. \quad .. \quad .. \quad .. \quad .. \quad .. \quad (3)$$

or

$$\{m\} = [s]\{\alpha\} . \quad .. \quad .. \quad .. \quad .. \quad .. \quad .. \quad .. \quad (4)$$

Premultiplication of equation (2) by $[s]$ gives, when compared with equation (4)

$$[s]\,[a] = I , \quad .. \quad .. \quad .. \quad .. \quad .. \quad .. \quad (5)$$

or

$$\begin{bmatrix} s_{11} & s_{12} \\ s_{21} & s_{22} \end{bmatrix} \begin{bmatrix} a_{11} & a_{12} \\ a_{21} & a_{22} \end{bmatrix} = \begin{bmatrix} 1 & 0 \\ 0 & 1 \end{bmatrix} . \quad .. \quad .. \quad .. \quad .. \quad (6)$$

The set of equations (6) enables the stiffnesses to be determined.

If σ is the stiffness relating to the reference section, it follows from consideration of the storage of elastic energy that

$$\begin{aligned} \tfrac{1}{2}\sigma\alpha_1^2 &= \tfrac{1}{2}(s_{11}\alpha_1 + s_{12}\alpha_2)\alpha_1 + \tfrac{1}{2}(s_{21}\alpha_1 + s_{22}\alpha_2)\alpha_2 \\ &= \tfrac{1}{2}(s_{11}\alpha_1^2 + 2\,s_{12}\alpha_1\alpha_2 + s_{22}\alpha_2^2) , \quad .. \quad .. \quad .. \quad .. \quad (7) \end{aligned}$$

since the cross-stiffnesses s_{12}, s_{21} are equal.

Hence

$$\sigma = s_{11} + 2s_{12}k + s_{22}k^2 , \quad .. \quad .. \quad .. \quad .. \quad .. \quad .. \quad (8)$$

where $k = \alpha_2/\alpha_1$. Values of k were determined experimentally for pitching oscillations in the manner described in the following section. The variation in σ for the maximum variation in k was of order $0{\cdot}5$ per cent.

It is assumed in the above analysis that the displacements at the ends of the model are in phase during an oscillation, and that the twist is linear.

In the case of torsional oscillations the stiffness used was that obtained by a static measurement with the bearing at station 2 clamped.

4. *Measurement of Mode.*—For the purpose of measuring the twist in the aerofoil during a pitching oscillation a small concave mirror was attached to each of the bearing cylinders and arranged to throw an image of an illuminated slit on to a white screen. With the aerofoil oscillating in still air the maximum displacements of the two oscillating images were observed simultaneously against scales on the screen. The ratio of these displacements gave a value for k as defined in the previous section.

Since it was necessary for the boxes to be closed when running the tunnel it was not possible to measure modes for this condition. The value of k used in the working out of results was that appropriate to the corresponding still-air oscillation, and the modes for both pitching and torsional oscillation tests were assumed to be linear.

The values of k related to still-air frequency f_0 are tabulated below:—

f_0	k
8·40 c.p.s.	0·781
10·47 ,,	0·787
13·14 ,,	0·798
16·36 ,,	0·816

5. *Amplitude Calibration.*—Each photographic record included a rough amplitude calibration obtained with the tunnel idle. With the film in motion in the camera, the model was rapidly deflected from its mean position to the position set by the collar K on the plunger D (Fig. 8). The angle of this deflection was known from the amount the plunger could be depressed after making contact with the arm A (Fig. 2).

6. *Analysis of Motion.*—6.1. *Formulae for Derivative Coefficients.*—The equation of motion of the system may be written

$$I\ddot{\alpha} + \varkappa\dot{\alpha} + \sigma\alpha = M_a, \quad .. \quad .. \quad .. \quad .. \quad .. \quad (9)$$

where

α is angular displacement,

σ stiffness,

I still-air moment of inertia,

$\varkappa$ apparatus damping factor,

M_a aerodynamic moment,

related to the reference section. The moment M_a may be expressed in the form

$$M_a = M_a\alpha + M_{\dot{a}}\dot{\alpha} + M_{\ddot{a}}\ddot{\alpha}, \quad .. \quad .. \quad .. \quad .. \quad .. \quad (10)$$

in which M_a, $M_{\dot{a}}$ and $M_{\ddot{a}}$ are the direct stiffness, damping and acceleration derivative coefficients respectively for pitching motion. In the present case they represent the total change in aerodynamic moment on the system when the tunnel is running.

The appropriate solution of equation (9) may be written in the form

$$\alpha = \alpha' e^{\lambda t}, \qquad (11)$$

where

$\lambda = \mu + jp$,
t is time,
α' is displacement when $t = 0$ (real part of equation (11)),
$p = 2\pi f$,
f is frequency of oscillation,
μ relates to rate of growth or decay,
$j = \sqrt{-1}$.

Substitution of equation (11) in equations (9) and (10) gives, on equating real and imaginary parts

$$(\mu^2 - p^2)M_{\ddot{a}} + \mu M_{\dot{a}} + M_a = (\mu^2 - p^2)I + \mu\varkappa + \sigma, \qquad (12)$$

$$2\mu M_{\ddot{a}} + M_{\dot{a}} = 2\mu I + \varkappa, \qquad (13)$$

from which follows

$$-(\mu^2 + p^2)M_{\ddot{a}} + M_a = -(\mu^2 + p^2)I + \sigma. \qquad (14)$$

With no wind in the tunnel equations (13) and (14) become

$$2\mu_0 I + \varkappa_0 = 0, \qquad (15)$$

$$(\mu_0^2 + p_0^2)I - \sigma = 0, \qquad (16)$$

the suffix 0 indicating values corresponding to this condition. The change in the apparatus damping factor from $\varkappa$ to $\varkappa_0$ is introduced in order to allow for the effect of change in frequency due to aerodynamic loading and change in air density. It is assumed that any change in I and σ with frequency and air density is negligible*.

Equations (13) to (16) lead to the relations

$$M_a - (p^2 + \mu^2)M_{\ddot{a}} = \{(p_0^2 + \mu_0^2) - (p^2 + \mu^2)\}I$$

$$= \sigma \frac{(p_0^2 + \mu_0^2) - (p^2 + \mu^2)}{p_0^2 + \mu_0^2}, \qquad (17)$$

$$M_{\dot{a}} + 2\mu M_{\ddot{a}} = 2\left(\mu - \frac{\varkappa}{\varkappa_0}\mu_0\right)I$$

$$= 2\sigma \frac{\mu - \frac{\varkappa}{\varkappa_0}\mu_0}{p_0^2 + \mu_0^2}, \qquad (18)$$

* Tests were made to determine the order of magnitude of the 'additional' still-air component of I by sealing-off the working-section with steel plates at top and bottom, and measuring the change in frequency on evacuation with a suction pump. Although a very accurate beat method of frequency measurement was employed, the effect was too small to be measurable.

which give the combinations of derivative coefficients on the left-hand side in terms of measurable quantities, provided a value for $\varkappa/\varkappa_0$ can be assigned.

6.2. *Apparatus Damping.*—It follows from equations (15) and (16) that, if μ_0^2 is negligible compared with p_0^2, which accords with the results of the tests, then

$$\varkappa_0 p_0 = -2\sigma\frac{\mu_0}{p_0} . \qquad .. \quad .. \quad .. \quad .. \quad .. \quad .. \quad (19)$$

The energy dissipation per cycle for a steady oscillation is proportional to $\varkappa p$, thus for hysteresis damping

$$\varkappa p = \text{const.} \qquad .. \quad .. \quad .. \quad .. \quad .. \quad .. \quad .. \quad (20)$$

Results of still-air oscillation tests, in which the variation with f_0 of $x_0 (= \pi\mu_0/p_0)$ was determined, showed that to the degree of experimental accuracy, x_0 could be regarded as constant, and thus from equation (19)

$$\varkappa_0 p_0 = \text{const.} , \qquad .. \quad .. \quad .. \quad .. \quad .. \quad .. \quad (21)$$

which indicates that the measurable apparatus damping was due to hysteresis. It follows that

$$\varkappa_0 p_0 = \varkappa p ,$$

or

$$\varkappa/\varkappa_0 = p_0/p . \qquad .. \quad .. \quad .. \quad .. \quad .. \quad .. \quad .. \quad (22)$$

6.3. *Approximate Formulae.*—A more convenient form for equations (17) and (18) is obtained by means of the substitutions $\mu = px/\pi$, $\mu_0 = p_0 x_0/\pi$, since x and x_0 are the slopes of logarithmic decrement curves obtained from analysis of records. In the resulting expressions x^2/π^2 and x_0^2/π^2 may be neglected in comparison with unity for all practical cases so far encountered.

The second term on the left-hand side of equation (17) represents the effect on aerodynamic moment of the change in additional inertia due to flow over the model, reduction of air density in the working section and cover boxes to the platforms, and to change in frequency of oscillation. It is assumed that, in the tests under discussion, these effects may be neglected in comparison with the aerodynamic stiffness. In equation (18) the corresponding term is neglected also, on the grounds of $M_{\dot{\alpha}}$ being small compared with I. The approximate equations for the reduction of the observations then become

$$M_\alpha = \sigma\frac{(f_0 + f)(f_0 - f)}{f_0^2} , \qquad .. \quad .. \quad .. \quad .. \quad .. \quad (23)$$

$$M_{\dot{\alpha}} = \sigma\frac{f^2 x - f_0^2 x_0}{\pi^2 f_0^2 f} , \qquad .. \quad .. \quad .. \quad .. \quad .. \quad .. \quad (24)$$

where the relation (22) and the substitutions $p = 2\pi f$, $p_0 = 2\pi f_0$ have been introduced.

6.4. *Analysis of Photographic Records.*—The trace on the photographic film may be represented by the equation

$$y = y' e^{\mu t} \cos pt + F(t) + C , \qquad .. \quad .. \quad .. \quad .. \quad .. \quad (25)$$

where y is displacement perpendicular to the direction of motion. $F(t)$ gives the effect of residual transient drift, and C allows for an arbitrary zero. Differentiation with respect to t leads to

$$\frac{dy}{dt} = y'e^{\mu t}(\mu \cos pt - p \sin pt) + \frac{dF(t)}{dt} . \quad .. \quad .. \quad .. \quad .. \quad (26)$$

If $dF(t)/dt$ is small compared with the greatest value of the preceding term, y has stationary values

$$y_s = (-1)^s A e^{sx} + F\left(t' + s\frac{\pi}{p}\right) + C , \quad .. \quad .. \quad .. \quad .. \quad (27)$$

where $\tan pt' = \mu/p$, $x = \pi\mu/p$, s is integral, and A is independent of s .

The rth order difference of y is given by

$$\Delta^r y_s = (-1)^{r+s} A(1 + e^x)^r e^{sx} + \Delta^r F\left(t' + s\frac{\pi}{p}\right) , \quad .. \quad .. \quad .. \quad .. \quad (28)$$

and if $F(t)$ can be represented by a polynomial in t of degree $r - 1$, then the second term on the right-hand side of equation (28) vanishes. Thus, if sign is ignored

$$\log_e \Delta^r y_s = sx + \text{const.} , \quad .. \quad .. \quad .. \quad .. \quad .. \quad (29)$$

which is a linear relationship between $\log_e \Delta^r y_s$ and s, in which the slope x is the logarithmic decrement with reversed sign.

For the purpose of analysis an enlarged image of the record was projected on to squared paper, and values of y_s were read off and related to s by plotting on the basis of equation (29). In practice it was found unnecessary to take differences of higher order than the second. Values of x obtained in this way relate to equation (24).

7. *Non-dimensional Derivative Coefficients.*

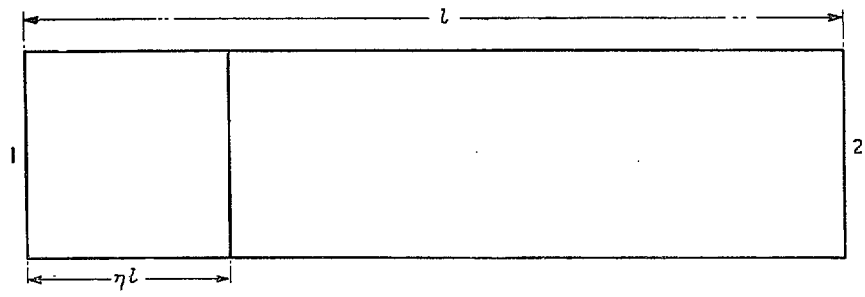

Consideration of the work done against aerodynamic forces when the reference section moves through a small angle $d\alpha$ leads to the relation

$$M_{\dot{\alpha}}\dot{\alpha}\, d\alpha = \rho c^3 l V m_{\dot{\alpha}}\dot{\alpha}\, d\alpha \int_0^1 f(\eta)^2\, d\eta ,$$

or

$$M_{\dot{\alpha}} = \rho c^3 l V m_{\dot{\alpha}} \int_0^1 f(\eta)^2\, d\eta , \quad .. \quad .. \quad .. \quad .. \quad .. \quad (30)$$

and similarly

$$M_a = \rho c^2 l V^2 m_a \int_0^1 f(\eta)^2 \, d\eta \, , \quad .. \quad .. \quad .. \quad .. \quad .. \quad .. \quad (31)$$

where

ρ is air density,
c chord,
l span,
V wind speed,
ηl spanwise distance from reference section,
α angular displacement at reference section (station 1),
$\alpha f(\eta)$ angular displacement at distance ηl from reference section,
$m_{\dot{\alpha}}$ non-dimensional damping derivative coefficient for pitching motion,
m_a non-dimensional stiffness derivative coefficient for pitching motion.

If the twist of the model is assumed to be linear and the angular displacement of the end remote from the reference section (station 2) is $k\alpha$, then

$$f(\eta) = 1 - \eta(1 - k) \, , \quad .. \quad .. \quad .. \quad .. \quad .. \quad .. \quad (32)$$

and

$$\int_0^1 f(\eta)^2 \, d\eta = \tfrac{1}{3}(1 + k + k^2) \, . \quad .. \quad .. \quad .. \quad .. \quad .. \quad (33)$$

Substitution of equation (33) in equations (30) and (31) leads to the relations

$$m_{\dot{\alpha}} = \frac{3M_{\dot{\alpha}}}{\rho c^3 l V (1 + k + k^2)} \, , \quad .. \quad .. \quad .. \quad .. \quad .. \quad (34)$$

$$m_a = \frac{3M_a}{\rho c^2 l V^2 (1 + k + k^2)} \, , \quad .. \quad .. \quad .. \quad .. \quad .. \quad (35)$$

which give the non-dimensional coefficients in terms of the derivative coefficients obtained from the relations (23) and (24), and the mode of oscillation represented by k and measured as described in section 4. For a torsional oscillation of the model $k = 0$.

8. *Experimental Results.*—The tests were carried out at a mean incidence of 0 deg and the deflection from which the model was released was 4 deg for the pitching and 2 deg for the torsional mode measured at the reference section, with the exception of a few observations at subsonic speeds for which growing oscillations building up from 0 deg amplitude were obtained. The non-dimensional derivative coefficients depend on the following non-dimensional parameters:—

$\omega = cp/V$ frequency parameter,
$\Omega = c\mu/V$ decay parameter,
$R = cV/\nu$ Reynolds number,
$M = V/a$ Mach number,

where

ν is kinematic viscosity,
a velocity of sound in the free stream,

the remaining symbols having been defined previously. No attempt was made to control Ω, and R varied with Mach number and the pressure and temperature at the tunnel intake. The values of Ω arising in the tests are given in the tables of derivative coefficients, whilst the variation of R with Mach number for standard intake conditions is given in Table 9. The frequency parameter ranged from 0 to a maximum of approximately 0·03, the very low value of which is due to the high wind speeds and small chord. Mach number could be varied continuously up to approximately $M = 0{\cdot}9$ at subsonic speeds, but only three supersonic values were obtainable, with effusers giving approximately $M = 1{\cdot}28$, $1{\cdot}46$ and $1{\cdot}52$.

8.1. *Supersonic Test Results for m_α and $m_{\dot{\alpha}}$.*—Values of $m_{\dot{\alpha}}$ and m_α are given in Tables 1 to 3 and in Figs. 11 to 16 for average Mach numbers of $1{\cdot}275$, $1{\cdot}455$ and $1{\cdot}515$ for both pitching and torsional modes. If due allowance is made for experimental scatter it appears that in all cases the variation with ω is negligible for the range covered. The damping derivative coefficient $m_{\dot{\alpha}}$ is negative in sign and decreases numerically with increase in Mach number. A similar trend of smaller magnitude is observed in the case of the stiffness derivative coefficient m_α which is positive in sign. The results for pitching and torsional modes of oscillation are in good agreement.

The logarithmic decrement curves for pitching oscillations at $M = 1{\cdot}275$ showed a more or less pronounced discontinuity of slope at a point corresponding on the average to an amplitude of $1{\cdot}4$ deg. A good example of this is shown in Fig. 17. A continuous drop in frequency with decreasing amplitude also occurred of the order 3 or 4 per cent. In such cases two values of the derivative coefficients have been obtained relating to the average conditions over the earlier and latter parts of the record respectively. This applies also to the stiffness derivative coefficients for pitching oscillations at $M = 1{\cdot}455$ for which a similar change in frequency of order 1 or 2 occurred. No change of slope in the logarithmic decrement curves was present in this case, and the damping derivative coefficients were based on the average frequency over the whole record.

The experimental scatter in Figs. 11 to 16 is greater for $M = 1{\cdot}275$ than for the other Mach numbers and is especially large in the case of $m_{\dot{\alpha}}$. It is considered that the errors in measurement were not large enough to account for this. On the other hand, there appears to be no correlation with variations in Mach number or wind velocity due to humidity changes, although these variations are quite appreciable. The results of two consecutive tests, the first with the tunnel wet and the second with the tunnel relatively dry, are included in Figs. 11 and 14, but show no remarkable difference. Rough measurements of the relative humidity at the tunnel intake were made during these tests, the values being 40 and 20 per cent respectively. This is certainly a greater difference than for the rest of the tests, since it is normal practice to dry the tunnel by running for some time before taking measurements, in order to allow the expanded air from the compressed-air containers to replace the air originally in the tunnel. By this means a relative humidity of from 15 to 20 per cent is obtainable.

8.2. *Comparison of Supersonic Results with Theory.*—Theoretical curves* showing the variation of $m_{\dot{\alpha}}$ and m_α with M when ω tends to zero are given in Figs. 18 and 19. These curves relate to theories of supersonic flutter derivatives by Temple and Jahn[1], by Collar[2], and by W. P. Jones[3]. Collar's theory is a simple approximate treatment which converges towards the Temple-Jahn theory as M tends to infinity. The variation of $m_{\dot{\alpha}}$ and m_α with ω is zero on the Collar theory and negligible over the range of the experiments on the Temple-Jahn theory. The treatment by Jones uses results derived from the Temple-Jahn theory in conjunction with Busemann's second order theory for steady motion, and takes into account the shape of the profile. It applies only for values of ω tending to zero.

* Theoretical values of m_α given in this report strictly include the term $-\omega^2 m_{\ddot{\alpha}}$, but this is negligible for the very small values of ω attained in the tests.

Three experimental points are included in Figs. 20 and 21 representing average values of the measurements of $m_{\dot{\alpha}}$ and m_{α} at $M = 1{\cdot}275$, $1{\cdot}455$ and $1{\cdot}515$. The results in Fig. 20 correspond to positive damping and show a large discrepancy with theory, especially when compared with the Temple-Jahn curve which indicates a change in sign of damping from positive to negative at Mach numbers below $M = \sqrt{2}$*. Apart from magnitude, the sign and trend with M of the experimental results agree with the curves due to Collar and W. P. Jones. Comparison with theoretical results is also given in Figs. 11, 12 and 13.

Two points are included in Fig. 20 showing the effect which the amount of flexure present in the experimental system would have on the measured value of $-m_{\dot{\alpha}}$ assuming the W. P. Jones derivatives to be correct. The result is an upward displacement of the curve which, although appreciable, is not nearly great enough to account for the discrepancy. The Temple-Jahn and Collar theories would give no effect due to flexure, since the cross-derivatives tend to zero for small values of ω. It should be remarked that inertial couplings are absent since the model is symmetrical about the axis.

The value of the stiffness derivative coefficient m_{α} is zero by Collar's theory and negligibly small over the experimental range according to Temple and Jahn. This results from the fact that both theories are linearized treatments of an infinitely thin flat aerofoil and predict a centre of pressure at the mid-chord position when ω tends to zero. When $\omega = 0$ static theory may be used, and a point is included in Figs. 15 and 21 based on the so-called 'exact' theory[4] applied to the profile under test. It is not possible to obtain a point for the lower Mach number $M = 1{\cdot}275$ since the theory then predicts a detached bow-wave followed immediately by subsonic flow for a semi-angle at the leading edge equal to that of the model (8 deg 34 min).

Application of Busemann's second-order theory[5] to the bi-convex profile leads to the formula

$$m_{\alpha} = \tfrac{2}{3} r C_2 \qquad \ldots \qquad (36)$$

where r is the thickness/chord ratio and C_2 is Busemann's second order coefficient given by

$$C_2 = \frac{1{\cdot}2M^4 - 2M^2 + 2}{(M^2 - 1)^2}. \qquad \ldots \qquad (37)$$

Results calculated from equations (36) and (37) are included in Figs. 14, 15, 16 and 21. The theory due to W. P. Jones gives the same result as Busemann for m_{α}. Experimental points derived from static pitching moment measurements made by Hilton[6] are also included. The trend with M of the measured values of m_{α} is shown in Fig. 21 and agrees with the Busemann and W. P. Jones theories. In magnitude, however, the experimental results are high, the discrepancy being greater for the oscillatory measurements than for the static results of Hilton.

It is fairly clear from the above results that a linear theory which takes no account of profile is inadequate for dealing with supersonic derivatives related to the half-chord axis. The large discrepancy between experiment and theory at $M = 1{\cdot}275$ in the case of $m_{\dot{\alpha}}$ may possibly be due to a detached bow-wave, but disagreement is still large at $M = 1{\cdot}455$ and $1{\cdot}515$ where the bow-wave is attached. A possible source of error in the experiments is tunnel wall interference due either to reflected shock-waves falling on the model or to the existence of regions of subsonic flow extending from the model to the tunnel walls as described by Hilton[7]. At the higher Mach number the latter effect would not be expected and the former only near the ends of the model. Static tests carried out to explore these effects at $M = 1{\cdot}275$ are described below.

---

* Positive $m_{\dot{\alpha}}$ corresponds to negative damping and would give rise to growing oscillations.

8.3. *Static Pressure Explorations.*—These tests were carried out with the model stationary and clamped. Traverses parallel to the direction of the free stream were made near the lower surface* of the model at mid-span and quarter-span positions as shown in Figs. 18, 19 and 22, and at three points near the tunnel wall on the same side of the model as indicated in Figs. 23 to 25. The different traverse positions were reached by means of a radial sliding mechanism which was set in one of three angular positions denoted by I, II, III as indicated in the diagrams. Positions along traverse lines are given as distances downstream from the leading edge. The flow is subsonic for all points above the horizontal dotted lines in the diagrams.

The curves in Figs. 18 and 22 show clearly the shock-wave from the leading edge and Fig. 19 shows the trailing-edge shock, but there is no indication of a shock-wave reflected back on to the model over the range of incidence covered. At 0 deg incidence the flow has just become sonic near the leading edge and at 4 deg a subsonic region extends from the leading edge approximately to the quarter-chord position.

Figs. 23 to 25 show the bow-wave striking the tunnel wall and its displacement with change of incidence. Fig. 25 also shows the trailing-edge shock. It is clear from these diagrams that subsonic regions of flow exist at the tunnel wall for all incidences at position I near the end of the model and at position III almost directly opposite the centre of the span. At position II, however, approximately mid-way between III and the position at the opposite end of the aerofoil corresponding to I the flow remains supersonic until an incidence of about 1·5 deg is reached. If this result is considered in relation to the logarithmic decrement curves exemplified by Fig. 17, it might be agreed that the change in slope which occurs for amplitudes above approximately 1·5 deg is due to the completion of a subsonic region of flow extending round the wall of the tunnel from one end of the model to the other. This, however, does not provide an explanation of the discrepancy between the theoretical and experimental values of $m_{\dot{\alpha}}$, since it would indicate a decrease in damping due to subsonic wall interference.

The failure to observe a reflected shock-wave falling on the model is explained by the presence of subsonic regions at the wall of the tunnel since no reflection occurs when the flow becomes subsonic. At small incidences reflections occurring in the supersonic region around position II would pass well behind the model since the bow-wave strikes the tunnel wall just ahead of the trailing-edge position.

8.4. *Subsonic Test Results for m_α and $m_{\dot{\alpha}}$.*—The subsonic measurements of m_α and $m_{\dot{\alpha}}$ were carried out for the pitching mode, and the model was released from a deflection of 4 deg with the exception of a few tests in which oscillations building up from 0 deg were obtained. Values of $m_{\dot{\alpha}}$ and m_α are given in Tables 4 to 7 and Figs. 26 to 29 for Mach numbers ranging from 0·4 to 0·9.

In the case of release from 4 deg some doubt existed as to the correct Mach number to apply to the results since this increased over a period of a few seconds immediately after release, due presumably to a difference in blocking effect between a stationary deflected model and an oscillating model. The maximum drift observed was of the order 5 per cent, but the changes were somewhat erratic, no doubt on account of tunnel unsteadiness. It was decided finally to use the Mach number reading taken immediately prior to release, in the hope of obtaining greater consistency between results.

The variation of $m_{\dot{\alpha}}$ and m_α with ω is shown in Figs. 28 and 29 for Mach numbers of 0·4, 0·6, 0·7 and 0·9. There appears to be little variation over the range covered. Measurements between $M = 0·7$ and $M = 0·8$ were unobtainable on account of an apparent divergence of the system which was characterised by the model on release swinging through the zero incidence position and attaining a negative deflection sufficient to trip the automatic brake.

* Since the tunnel is vertical this is taken to be the surface subject to a pressure increase when the model is given a positive incidence.

Variation with Mach number over the whole range from 0·4 to 0·9 is shown in Figs. 26 and 27, in which each curve relates to a particular still-air natural frequency of the system. The damping derivative coefficient $m_{\dot{\alpha}}$ remains practically constant up to $M = 0{\cdot}6$ after which it increases rapidly in numerical value until at $M = 0{\cdot}8$ it is approximately ten times its initial value in the case of the lowest natural frequency (Fig. 26). Between $M = 0{\cdot}8$ and 0·9 a sharp drop occurs, with a change in sign between $M = 0{\cdot}87$ and 0·89 approximately. In this region the damping is negative and growing oscillations of the aerofoil were obtained on release. Beyond $M = 0{\cdot}89$ the damping becomes increasingly positive. The rise in damping between $M = 0{\cdot}6$ and 0·8 becomes less rapid the higher the natural frequency of the system, but the sudden drop does not alter in character. A few points are included in Fig. 26 which correspond to growing oscillations released from 0 deg incidence.

There appeared to be considerable amplitude effects and fluctuations in damping at the higher Mach numbers, so that points plotted were necessarily derived from average slopes of logarithmic decrement curves. Release from 0 deg incidence in the range $M = 0{\cdot}87$ to 0·89 gave rise either to an oscillation growing indefinitely, or to one which grew to a sustained but fluctuating amplitude. In the latter case the damping at the average amplitude of the oscillation has been assumed equal and opposite to the apparatus damping.

The stiffness derivative coefficient m_{α} exhibits a gradual rise in value up to a Mach number of 0·8 followed by a sudden drop to about one-quarter of its maximum value in the region of $M = 0{\cdot}88$, which corresponds to the drop in the damping curve (Fig. 27). There is indication of a rise following further increase in Mach number. The natural frequency of the system appears to have little effect in this case. A number of points derived from static measurements made by Hilton[6] are included in Figs. 29 and 27.

The variation of ω along the curves in Figs. 26 and 27 is shown in Fig. 30. On account of the rapid change of the derivative coefficients with Mach number in the region 0·8 to 0·9, no curves are given showing variation with ω over this range since in general they would be vitiated by Mach number errors. Where the trend is unmistakable it can be observed from a comparison of Figs. 26 and 27 with Fig. 30.

An approximate calculated critical Mach number for the profile under test is $M = 0{\cdot}83$, which suggests that a physical explanation of the sudden changes in the derivative coefficients is probably to be found in the formation of a shock-wave at the surface of the model, possibly followed by separation of flow. On this assumption it would appear that the observed instability is related to the phenomenon of aileron buzz[8] in which a shock-wave formed at the surface of a wing ahead of the aileron produces unstable oscillations of the latter. The present case differs in so far as the shock-wave would be formed at the surface of the oscillating body. Experimental evidence for the formation of shock-waves at the relevant Mach number is furnished by drag measurements made by Hilton[6] which show a steep rise at approximately $M = 0{\cdot}875$. The possibility of the unstable oscillations being due to so-called classical flutter involving flexure of the model appears to be ruled out by the fact that the critical speed is independent of the natural pitching frequency.

A comparison between the oscillatory subsonic experimental results of Figs. 26 and 27, and the supersonic results of Figs. 18 and 19 is given in Figs. 31 and 32.

8.5. *Sustained or Growing Oscillations at Subsonic Speeds.*—Further tests were carried out in the region $M = 0{\cdot}86$ to 0·91 in order to obtain additional information on the sustained or growing oscillations mentioned above. In these tests the model was released from 0 deg incidence and the oscillation allowed to build up. In general, the amplitude of the resulting sustained oscillation fluctuated considerably, and only a rough estimate of the average value was obtained by observing the length of the trace on the cathode-ray oscillograph. The accuracy, however, was sufficient to show the form of variation of amplitude with Mach number and frequency.

The results are shown in Figs. 33 and 34 for pitching and torsional oscillations respectively. The curves given in these figures show the variation with M of sustained amplitude for different values of the still-air natural frequency, and all exhibit the same general form of a rise from zero followed by a fall to zero with increasing Mach number. In some cases the maximum value lay outside the experimental range. Points situated below such a curve correspond to net negative damping on the system.

In the case of the pitching mode the effect of increase in natural frequency is to displace the curve bodily in the direction of decreasing Mach number. For the torsional mode, however, the position on the Mach number scale appears to remain unchanged, but the height of the curve is reduced. At the highest torsional frequency the curve is completely flattened and no sustained oscillations are obtained. The difference in behaviour between the two modes is presumably associated with difference in lift distribution.

The effects described in this section appeared to be very sensitive to atmospheric conditions, and in order to obtain consistent results the tests had to be completed in a short space of time. It is probably for this reason that the corresponding points in Fig. 26 and Table 8 do not agree well with Figs. 33 and 34.

8.6. *Comparison of Subsonic Results with Theory.*—The full curves included in Fig. 28 are approximations to theoretical subsonic damping derivative coefficients for small values of ω obtained by W. P. Jones, whilst the broken curves represent values derived from the results of incompressible flow theory by introduction of the Glauert factor $1/(1 - M^2)^{1/2}$. In the case of the stiffness derivative coefficient, the two treatments give identical results and are represented by full lines in Fig. 29. The double circles in Figs. 26 and 27 relate to subsonic theory for the lowest natural frequency of the system.

The experimental values of $-m_{\dot{\alpha}}$ are low compared with theory over the range $M = 0{\cdot}4$ to $0{\cdot}7$. Above this value of Mach number violent changes with ω occur in the experimental results which are not exhibited by theory. The experimentally determined values of m_{α} agree reasonably well with theory up to $M = 0{\cdot}8$. In neither case does the theoretical treatment predict the sudden fall in value observed in the region $M = 0{\cdot}87$. It should be remarked that the profile tested had a sharp leading edge, which may account for the discrepancy between experiment and theory at the lower Mach numbers.

Acknowledgments.—The authors wish to express their indebtedness to the Staff of the High Speed Laboratory, Aerodynamics Division, N.P.L., who gave valuable help and advice throughout the course of the tests.

REFERENCES

No.	*Author*	*Title, etc.*
1	G. Temple and H. A. Jahn ..	Flutter at Supersonic Speeds. Derivative Coefficients for a Thin Aerofoil at Zero Incidence. R. & M. 2140. April, 1945.
2	A. R. Collar	Resistance Derivatives of Flutter Theory. Part II: Results for Supersonic Speeds. R. & M. 2139. January, 1944.
3	W. P. Jones	The Influence of Thickness/Chord Ratio on Supersonic Derivatives for Oscillating Aerofoils. R. & M. 2679. September, 1947.
4	M. J. Lighthill..	Two-dimensional Supersonic Aerofoil Theory. R. & M. 1929. January, 1944.
5	A. Busemann	Aerodynamic Lift at Supersonic Speeds. (Lecture given at the 5th Volta Conference at Rome). (*L.F.F.*, Vol. 12, No. 6, 3.10.35). Translated by W. J. Stern, A.R.C.S. A.R.C. 2844. February, 1937.
6	W. F. Hilton	Subsonic and Supersonic Tests on a $7\frac{1}{2}$ per cent Bi-convex Aerofoil. R. & M. 2196. May, 1944.
7	W. F. Hilton	Note on Two-dimensional Supersonic Tunnel Interference. R. & M. 2332. December, 1943.
8	B. Smilg	Prevention of Aileron Oscillations at Transonic Airspeeds. (Presented at 6th International Congress for Applied Mechanics, Paris, September 25th, 1946). Advance Copy of Army Air Forces Technical Report No. 5530. Communicated by the Director of Aircraft Research and Development, Ministry of Supply. A.R.C. 10,115. November, 1946. (Unpublished.)

TABLE 1

Supersonic Flow

Values of $m_{\dot{\alpha}}$ and m_{α} for $M = 1 \cdot 275$ (mean value)

α' deg	f c.p.s.	$-\Omega \times 10^6$	M	ω	$-m_{\dot{\alpha}}$	m_{α}	
3·4 — 0·7	7·20	14·3	1·305	0·00610	0·575	0·320	Pitching
	7·00	13·9		0·00590		0·369	
3·1—1·6—0·5	7·25	13·5	1·290	0·00620	0·542	0·311	
	7·06	23·0		0·00605	0·984	0·358	
3·8—1·7—0·5	8·96	20·6	1·290	0·00765	0·544	0·324	
	8·72	24·0		0·00745	0·646	0·371	
4·0—1·4—0·5	8·99	19·3	1·295	0·00770	0·501	0·315	
	8·69	25·4		0·00740	0·684	0·373	
3·5—1·3—0·4	8·97	19·2	1·300	0·00760	0·502	0·319	
	8·66	29·1		0·00735	0·801	0·378	
2·9—1·1—0·3	11·32	27·8	1·265	0·00975	0·469	0·312	
	11·78	36·0		0·00925	0·621	0·396	
2·7—1·1—0·4	11·27	30·4	1·290	0·00960	0·519	0·312	
	10·94	42·9		0·00930	0·748	0·363	
	14·02	43·6	1·305	0·01185	0·510	0·314	
	13·66	54·5		0·01155	0·639	0·358	
2·7—1·4—0·2	13·81	52·3	1·290	0·01175	0·591	0·333	
	13·40	68·9		0·01140	0·790	0·382	
1·8 — 0·7	13·04	9·4	1·265	0·01120	0·827	0·339	Torsion
1·8 — 0·7	13·08	8·2	1·270	0·01130	0·693	0·367	
1·7 — 0·7	16·38	12·6	1·270	0·01415	0·705	0·331	
1·9 — 0·7	16·38	12·2	1·260	0·01395	0·699	0·321	
1·7 — 0·5	20·78	18·7	1·265	0·01800	0·681	0·316	
1·9 — 0·6	20·81	15·5	1·270	0·01795	0·542	0·299	
1·8 — 0·4	26·21	27·0	1·260	0·02270	0·653	0·320	
1·7 — 0·3	26·21	26·5	1·260	0·02235	0·630	0·327	
3·5—1·5—0·3	11·28	29·8	1·290	0·00960	0·505	0·309 *	Pitching
	10·85	39·6		0·00925	0·683	0·374 *	
2·5—1·2—0·2	11·48	27·4	1·210	0·01020	0·434	0·285 †	
	11·04	39·7		0·00980	0·649	0·353 †	

α' indicates amplitude range analysed, and discontinuity when present.
* 20 per cent relative humidity.
† 40 per cent relative humidity.

TABLE 2

Supersonic Flow

Values of $m_{\dot{\alpha}}$ and m_{α} for $M = 1{\cdot}455$ (mean value)

α' deg	f c.p.s.	$-\Omega \times 10^6$	M	ω	$-m_{\dot{\alpha}}$	m_{α}	
3·3 — 0·7	7·45	7·3	1·450	0·00585	0·314	0·265	Pitching
	7·37			0·00580		0·285	
3·1 — 0·1	7·43	7·0	1·445	0·00590	0·285	0·262	
	7·37			0·00585		0·277	
3·4 — 1·1	9·29	10·6	1·470	0·00730	0·292	0·259	
	9·21			0·00725		0·275	
2·5 — 0·4	9·21	10·3	1·480	0·00710	0·291	0·268	
	9·13			0·00705		0·284	
2·3 — 0·2	11·53	17·4	1·480	0·00900	0·338	0·275	
	11·45			0·00895		0·288	
3·7 — 0·5	11·58	17·3	1·445	0·00910	0·333	0·269	
	11·44			0·00900		0·291	
2·0 — 0·2	14·28	26·1	1·430	0·01135	0·332	0·280	
	14·20			0·01130		0·290	
2·5 — 0·3	14·31	25·8	1·445	0·01130	0·329	0·276	
	14·18			0·01120		0·297	
1·7 — 1·0	13·14	4·6	1·485	0·01020	0·360	0·251	Torsion
1·5 — 0·9	13·14	4·8	1·420	0·01050	0·374	0·252	
1·4 — 0·8	16·47	6·4	1·485	0·01290	0·341	0·251	
0·4 — 0·2	20·86	9·8	1·440	0·01655	0·375	0·265	
1·3 — 0·7	20·87	9·8	1·440	0·01650	0·358	0·260	
1·0 — 0·4	26·33	13·8	1·475	0·02060	0·327	0·266	
1·1 — 0·5	26·35	13·4	1·480	0·02040	0·341	0·261	
1·1 — 0·3	26·33	14·0	1·445	0·02050	0·336	0·256	

α' indicates amplitude range analysed.

TABLE 3

Supersonic Flow

Values of $m_{\dot{\alpha}}$ and m_{α} for $M = 1{\cdot}515$ (mean value)

α' deg	f c.p.s.	$-\Omega \times 10^6$	M	ω	$-m_{\dot{\alpha}}$	m_{α}	
4·0 — 1·6	7·51	6·0	1·505	0·00560	0·246	0·242	Pitching
4·0 — 1·4	7·54	5·9	1·520	0·00560	0·249	0·237	
4·0 — 1·3	9·37	8·5	1·545	0·00690	0·243	0·245	
4·0 — 1·1	9·35	8·2	1·500	0·00700	0·216	0·242	
3·9 — 0·8	11·75	12·4	1·545	0·00865	0·237	0·240	
3·8 — 0·8	11·72	13·0	1·530	0·00870	0·251	0·247	
1·9 — 0·4	14·43	17·6	1·515	0·01080	0·212	0·256	
3·8 — 0·8	14·56	18·5	1·510	0·01095	0·228	0·243	
3·5 — 0·3	14·52	17·9	1·510	0·01095	0·209	0·246	
1·9 — 1·2	13·10	4·3	1·510	0·00975	0·391	0·253	Torsion
1·9 — 1·2	13·11	4·0	1·500	0·00980	0·348	0·254	
2·0 — 1·3	13·11	3·9	1·505	0·00970	0·343	0·253	
1·9 — 1·2	16·43	5·3	1·500	0·01230	0·306	0·252	
1·9 — 1·0	20·82	8·2	1·515	0·01540	0·329	0·253	
1·8 — 1·0	26·28	11·1	1·515	0·01940	0·285	0·254	
1·8 — 0·9	26·29	11·6	1·505	0·01965	0·291	0·254	

α' indicates amplitude range analysed.

TABLE 4

Subsonic Flow

Values of $m_{\dot{\alpha}}$ and m_α for a Natural Frequency 8·41 c.p.s.

α' deg	f c.p.s.	$-\Omega \times 10^6$	M	ω	$-m_{\dot{\alpha}}$	m_α
4·0 — 0·5	7·78	50	0·390	0·01910	1·145	0·780
3·2 — 0·3	6·81	45	0·597	0·01105	1·155	0·897
5·3 — 0·8	6·01	65	0·690	0·00840	1·860	1·020
2·7 — 0·3	4·97	375	0·811	0·00615	11·860	1·117
4·0 — 0·3	4·91	355	0·811	0·00605	11·260	1·141
3·9 — 0·4	5·02	246	0·842	0·00600	7·930	1·068
3·0 — 0·9	5·54	216	0·859	0·00650	7·020	0·912
3·0 — 0·3	6·25	245	0·861	0·00730	8·110	0·719
3·0 — 0·7	6·76	142	0·869	0·00780	4·690	0·564
2·8 — 0·8	6·21	260	0·869	0·00725	+8·530	0·725
1·0	7·59	0	0·880	0·00870	—0·080	0·292
2·5	7·68	0	0·880	0·00885	—0·080	0·261
3·1 — 0·5	7·28	25	0·898	0·00825	+0·765	0·384

α' indicates amplitude range analysed.

TABLE 5

Subsonic Flow

Values of $m_{\dot{\alpha}}$ and m_α for a Natural Frequency 10·47 c.p.s.

α' deg	f c.p.s.	$-\Omega \times 10^6$	M	ω	$-m_{\dot{\alpha}}$	m_α
3·9 — 0·6	9·53	72	0·418	0·02180	1·060	0·799
3·7 — 0·5	8·30	75	0·615	0·01315	1·240	0·914
4·7 — 0·5	7·40	103	0·691	0·01045	1·850	1·044
4·0 — 0·4	6·04	434	0·810	0·00745	8·850	1·154
3·8 — 0·7	5·81	411	0·814	0·00715	8·270	1·174
3·9 — 0·4	6·21	323	0·843	0·00735	6·820	1·070
4·0 — 0·6	7·03	354	0·862	0·00815	7·500	0·870
3·7 — 1·4	8·08	+165	0·872	0·00940	+3·420	0·637
3·8 — 4·6	8·60	— 50	0·882	0·00990	—1·150	0·504
3·6 — 0·7	9·07	+ 38	0·900	0·01025	+0·745	0·378

α' indicates amplitude range analysed.

TABLE 6

Subsonic Flow

Values of $m_{\dot{\alpha}}$ and m_α for a Natural Frequency 13·15 c.p.s.

α' deg	f c.p.s.	$-\Omega \times 10^6$	M	ω	$-m_{\dot{\alpha}}$	m_α
3·8 — 0·5	12·06	110	0·403	0·02870	1·045	0·792
3·7 — 0·3	12·04	111	0·406	0·02840	1·055	0·787
3·6 — 0·4	10·50	112	0·604	0·01700	1·185	0·915
3·7 — 0·3	10·50	114	0·612	0·01675	1·220	0·895
	9·34	165	0·693	0·01320	1·915	1·020
3·9 — 0·7	6·71	481	0·803	0·00950	6·030	1·136
3·3 — 0·4	7·64	393	0·819	0·00925	5·070	1·104
3·8 — 0·6	8·33	434	0·852	0·00985	5·680	0·955
3·3 — 0·7	8·96	+85	0·864	0·01045	+1·070	0·842
4·1 — 4·9	9·43	—76	0·873	0·01095	—1·065	0·755
4·1 — 0·9	11·40	+52	0·884	0·01310	+0·655	0·381
3·6 — 0·5	11·38	57	0·900	0·01295	0·725	0·378

α' indicates amplitude range analysed.

TABLE 7

Subsonic Flow

Values of $m_{\dot{\alpha}}$ and m_α for a Natural Frequency 16·36 c.p.s.

α' deg	f c.p.s.	$-\Omega \times 10^6$	M	ω	$-m_{\dot{\alpha}}$	m_α
3·9 — 0·2	14·84	161	0·425	0·03340	1·010	0·782
3·9 — 0·4	12·87	183	0·619	0·02030	1·275	0·910
3·9 — 0·6	11·51	256	0·693	0·01620	1·910	1·021
3·5 — 0·6	9·91	598	0·801	0·01235	4·810	1·070
3·8 — 0·5	9·85	608	0·823	0·01200	4·950	1·043
3·5 — 0·7	9·82	678	0·841	0·01175	+5·300	0·968
2·4	11·64	0	0·862	0·01365	—0·035	0·767
2·0	12·80	0	0·871	0·01490	—0·030	0·596
3·8 — 5·0	13·47	—59	0·882	0·01465	—0·560	0·488
3·8 — 0·6	14·19	+86	0·898	0·01610	+0·715	0·369

α' indicates amplitude range analysed.

TABLE 8

Subsonic Flow

Values of $m_{\dot{\alpha}}$ and m_{α} for Release from 0 deg Incidence

α' deg	f c.p.s.	f_0 c.p.s.	$-\Omega \times 10^6$	M	ω	$-m_{\dot{\alpha}}$	m_{α}
1·5	10·76	13·15	0	0·880	0·01230	—0·040	0·508
2·1	12·77	16·36	0	0·880	0·01460	—0·025	0·589
0 — max.	13·50	16·36	—18	0·885	0·01535	—0·160	0·478
0 — max.	9·22	10·47	—119	0·890	0·01045	—2·515	0·343
	11·96	13·15		0·890	0·01400		0·262
0 — max.	13·53	16·36	—13	0·890	0·01535	—0·110	0·471
1·6	7·60	8·41	0	0·895	0·00895	—0·070	0·283
	8·98	10·47		0·895	0·01045		0·402

f_0 indicates still-air natural frequency.

α' indicates sustained or growing oscillation (max. denotes brake tripped).

TABLE 9

Variation of Reynolds number with Mach number

N.P.L. circular H.S.T. 2-in. chord aerofoil. Standard intake conditions.

M	$R \times 10^{-6}$	M	$R \times 10^{-6}$
0·3	0·343	1·1	0·813
0·4	0·444	1·2	0·820
0·5	0·534	1·22	0·822*
0·6	0·612	1·3	0·820
0·7	0·678	1·4	0·813
0·8	0·730	1·5	0·800
0·9	0·770	1·6	0·774
1·0	0·797		

* Maximum R.

APPENDIX

Transient Effects in a Series Resistance-Capacity Circuit.

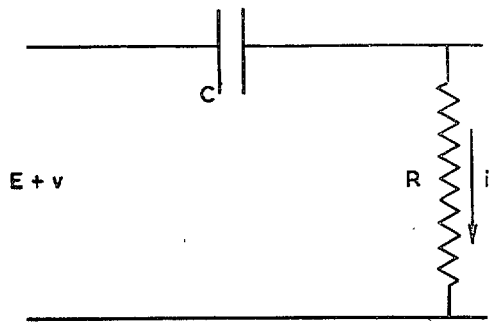

The circuit consists of a capacity C and resistance R in series, and the input voltage is $E + v$ where E is oscillatory and v is a steady voltage introduced at time $t = 0$ to represent the effect of shorting R_2 as described in section 2.3. It is assumed that the current i is zero immediately prior to the introduction of v, thus the initial value of i at time $t = 0$ is given by $i = v/R$.

The equation for the circuit is

$$(D + \gamma)i = \frac{1}{R} D(E + v) \qquad (1)$$

where D denotes d/dt and $\gamma = 1/RC$. If E is written in the form $E' e^{\lambda t}$, equation (1) becomes

$$(D + \gamma)i = \frac{E'}{R} \lambda e^{\lambda t} . \qquad (2)$$

and the operational solution is given by

$$(p + \gamma)\bar{i} = \frac{E'}{R} \cdot \frac{\lambda}{p - \lambda} + \frac{v}{R} \qquad (3)$$

where the bar denotes the Laplace Transform. From equation (3)

$$\bar{i} = \frac{E'}{R} \cdot \frac{\lambda}{\gamma + \lambda} \left(\frac{1}{p - \lambda} - \frac{1}{p + \gamma} \right) + \frac{v}{R} \cdot \frac{1}{p + \gamma} \qquad (4)$$

whence

$$i = \frac{E'}{R} \cdot \frac{\lambda}{\gamma + \lambda} (e^{\lambda t} - e^{-\gamma t}) + \frac{v}{R} e^{-\gamma t} \qquad (5)$$

where the terms involving $e^{-\gamma t}$ represent the transient drift.

If $\lambda = \mu + j\omega$, equation (5) becomes

$$i = \frac{E'}{R} \cdot \frac{\cos \varepsilon}{\cos \varepsilon'} \left\{ \begin{array}{l} e^{\mu t} \cos (\omega t + \varepsilon - \varepsilon') - e^{-\gamma t} \cos (\varepsilon - \varepsilon') \\ + j[e^{\mu t} \sin (\omega t + \varepsilon - \varepsilon') - e^{-\gamma t} \sin (\varepsilon - \varepsilon')] \end{array} \right\} + \frac{v}{R} e^{-\gamma t} \qquad (6)$$

where $\tan \varepsilon = (\gamma + \mu)/\omega$ and $\tan \varepsilon' = \mu/\omega$. The real part of equation (6) gives

$$i = \frac{1}{R}\left\{E' \frac{\cos \varepsilon}{\cos \varepsilon'} \cdot e^{\mu t} \cos (\omega t + \varepsilon - \varepsilon') + \left[v - E' \frac{\cos \varepsilon \cos (\varepsilon - \varepsilon')}{\cos \varepsilon'}\right] e^{-\gamma t}\right\} \quad .. \quad (7)$$

which corresponds to an input $E = E' e^{\mu t} \cos \omega t$. This is the case of release from a deflected position giving $E = E'$ at time $t = 0$, and the transient term vanishes if

$$v = E' \frac{\cos \varepsilon \cos (\varepsilon - \varepsilon')}{\cos \varepsilon'}$$

$$= E' \frac{1 + \tan \varepsilon \tan \varepsilon'}{1 + \tan^2 \varepsilon} \cdot \quad .. \quad .. \quad .. \quad .. \quad (8)$$

Hence if γ and μ are small, which corresponds to a large time constant CR and a small rate of growth or decay, equation (8) becomes, very nearly,

$$v = E' . \quad .. \quad .. \quad .. \quad .. \quad .. \quad .. \quad .. \quad (9)$$

The case of a growing oscillation released from its mean position is represented by $E = E' e^{\mu t} \sin \omega t$ with μ positive, and the solution is given by the imaginary part of equation (6). The transient term cannot now be neutralized in the way described above, but since it includes a factor $\sin (\varepsilon - \varepsilon')$ it will be small provided γ and μ are small.

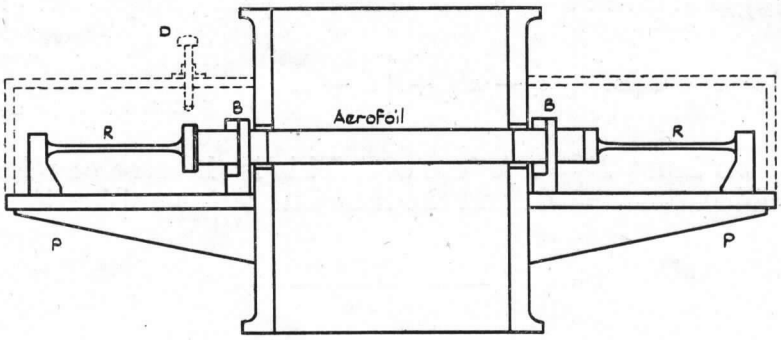

FIG. 1. Elevation of tunnel working-section.

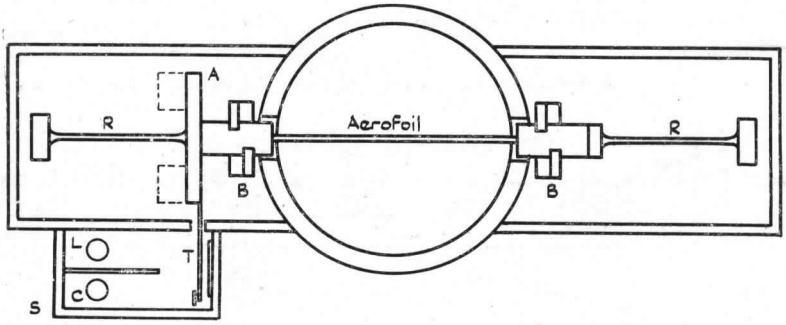

FIG. 2. Plan of tunnel working-section.

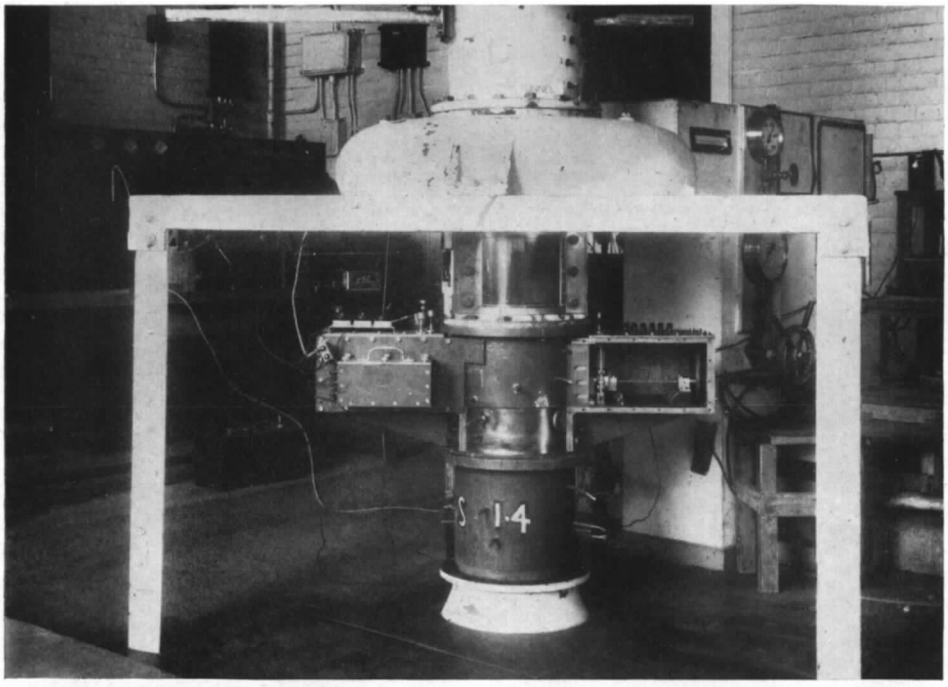

FIG. 3. View of tunnel working-section.

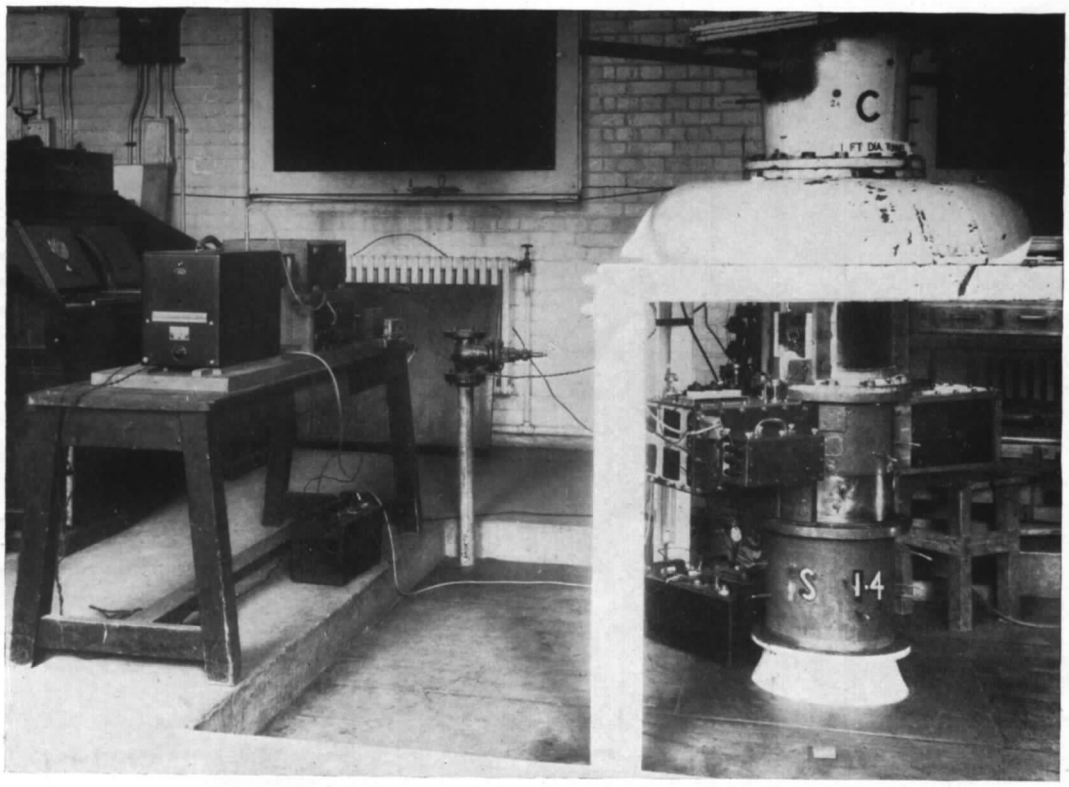

FIG. 4. Tunnel working-section and recording equipment.

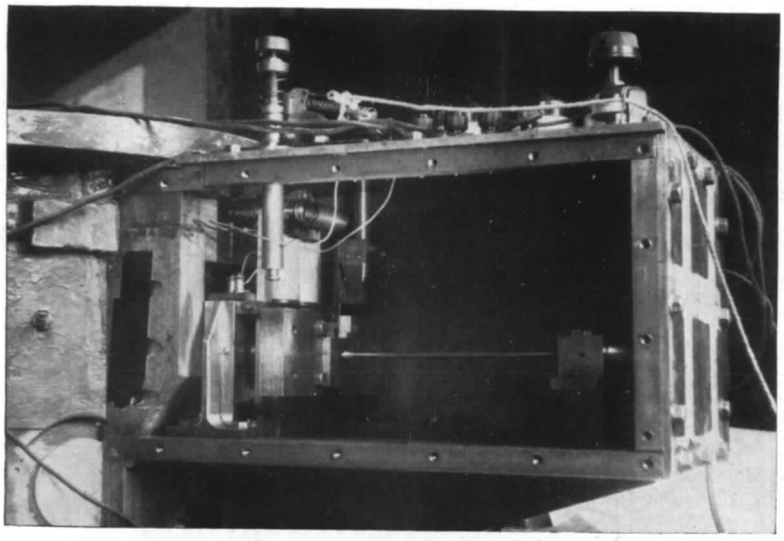

FIG. 5. View of side-box.

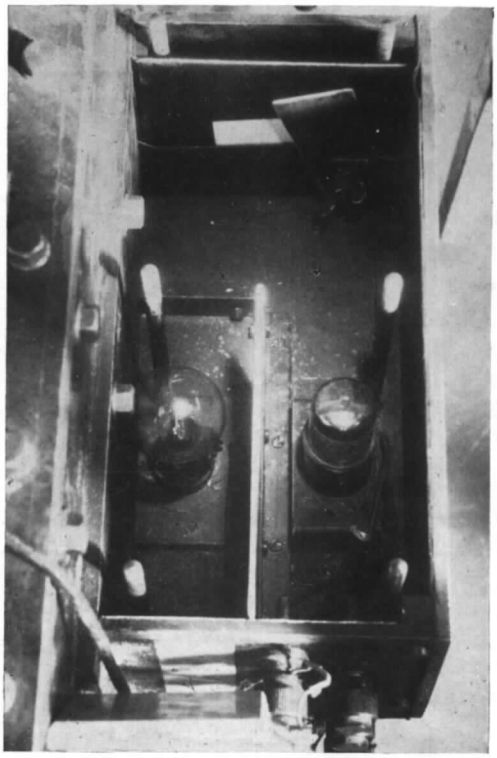

FIG. 6. Small side-box with recording mechanism.

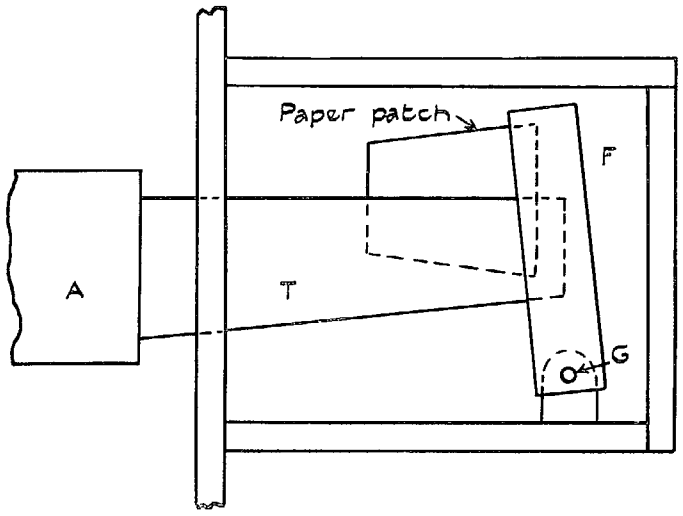

FIG. 7. Recording mechanism in side-box.

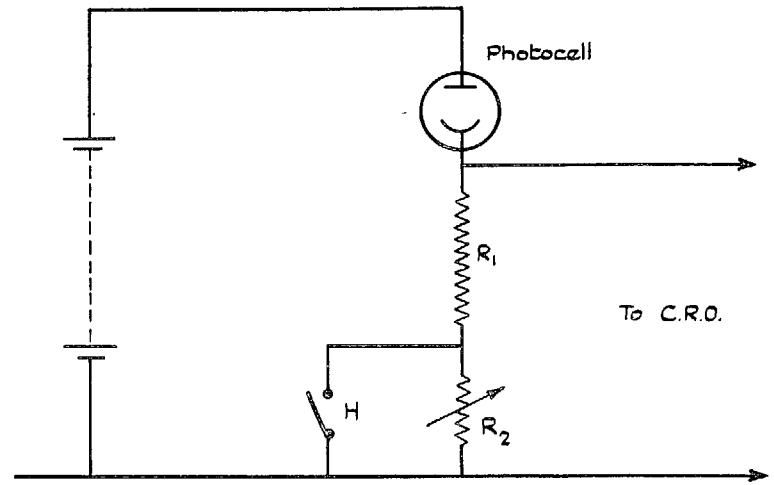

FIG. 9. Circuit diagram.

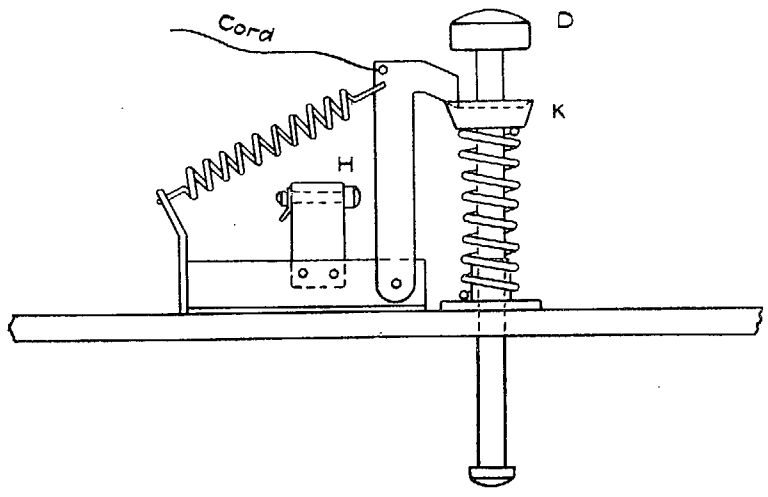

FIG. 8. Release mechanism.

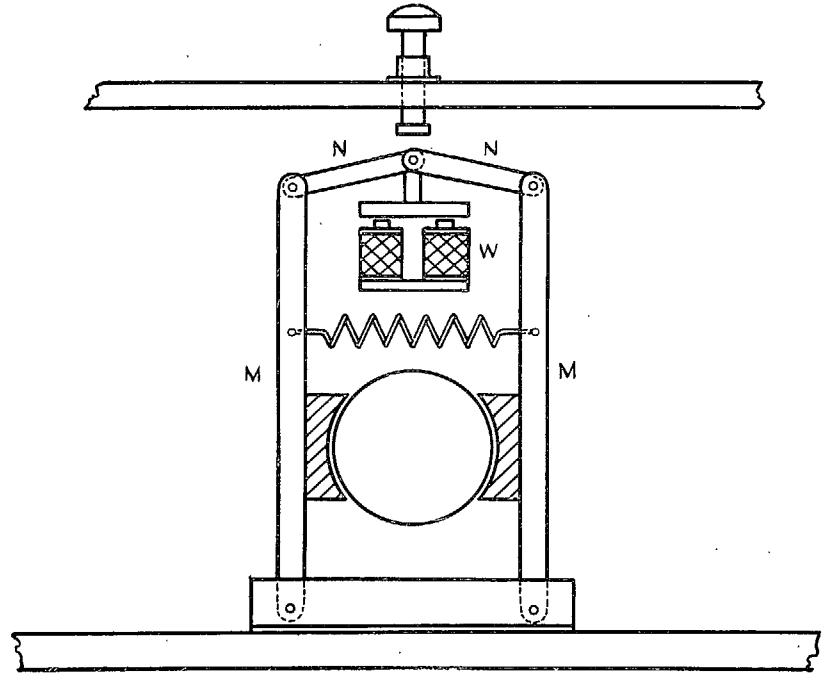

FIG. 10. Brake mechanism.

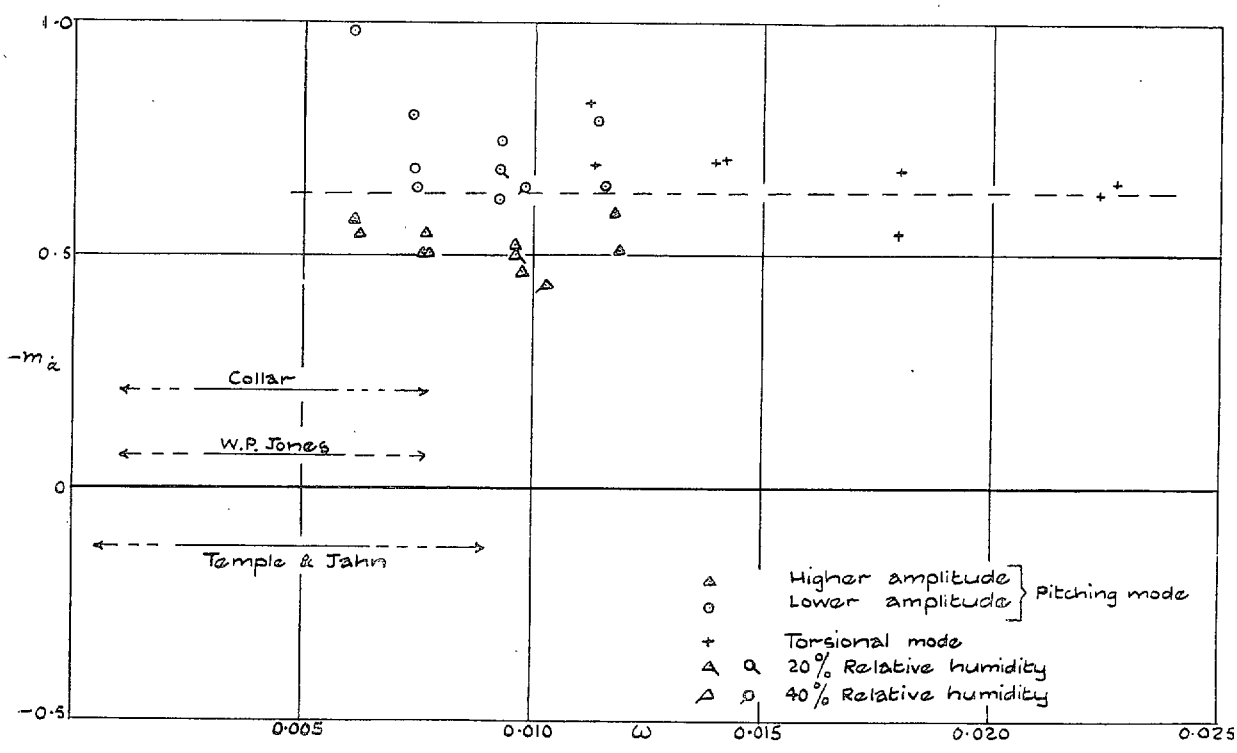

FIG. 11. Dependence of $-m_{\dot{\alpha}}$ on ω for $M = 1{\cdot}275$ (mean value).

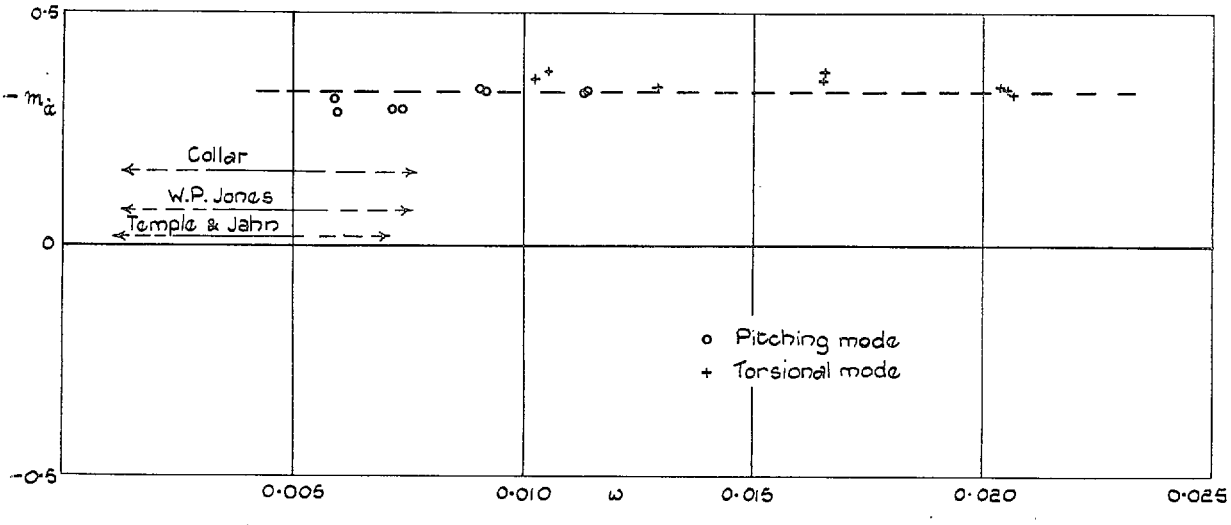

FIG. 12. Dependence of $-m_{\dot{\alpha}}$ on ω for $M = 1{\cdot}455$ (mean value).

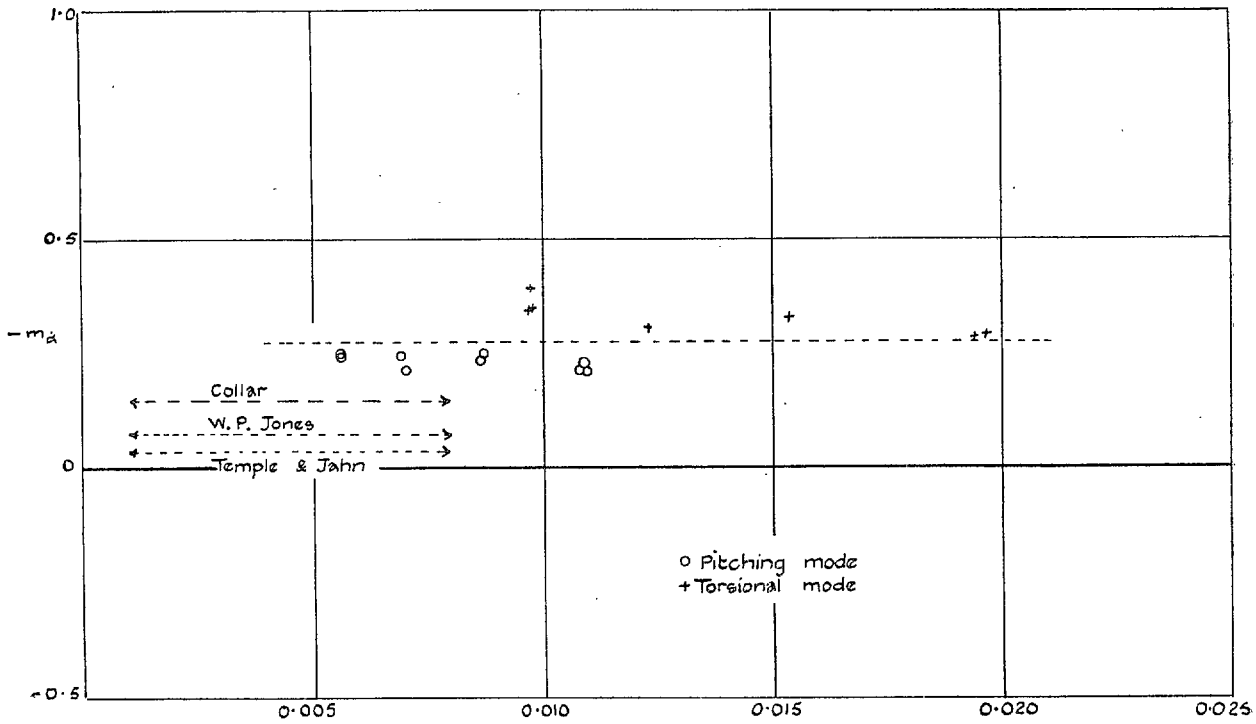

FIG. 13. Dependence of $-m_{\dot{\alpha}}$ on ω for $M = 1{\cdot}515$ (mean value).

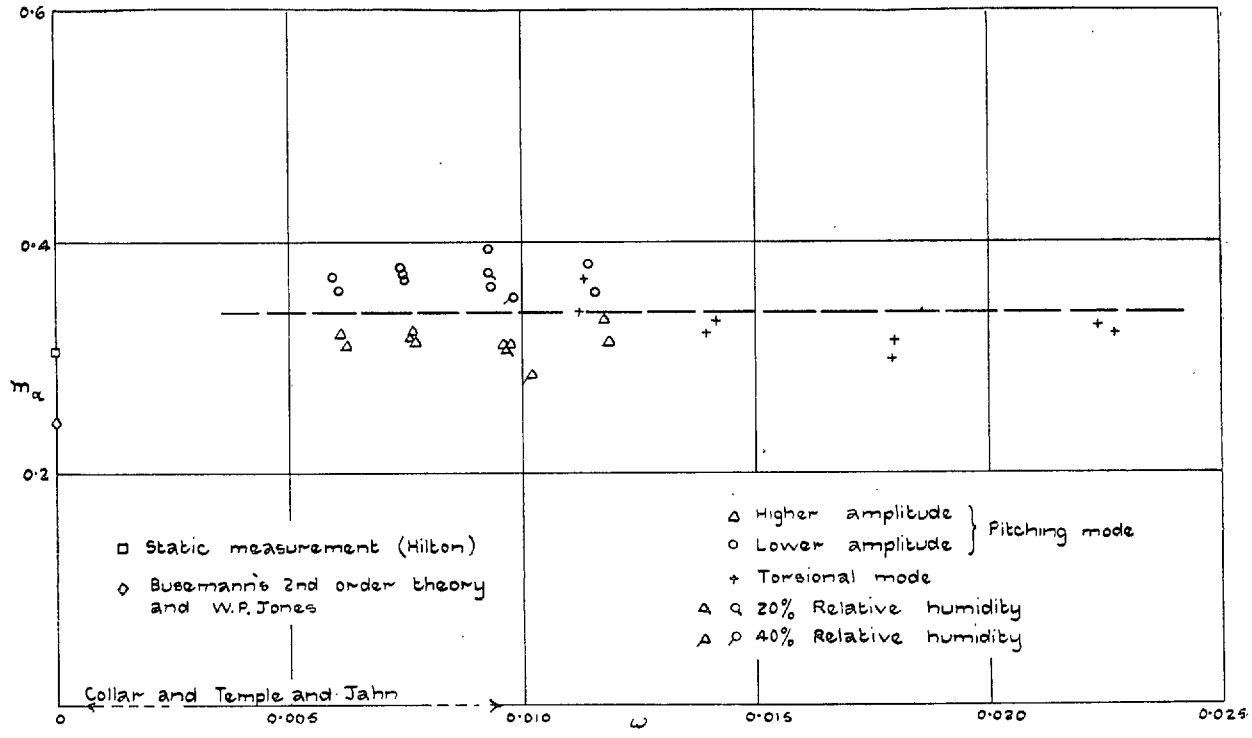

FIG. 14. Dependence of m_α on ω for $M = 1{\cdot}275$ (mean value).

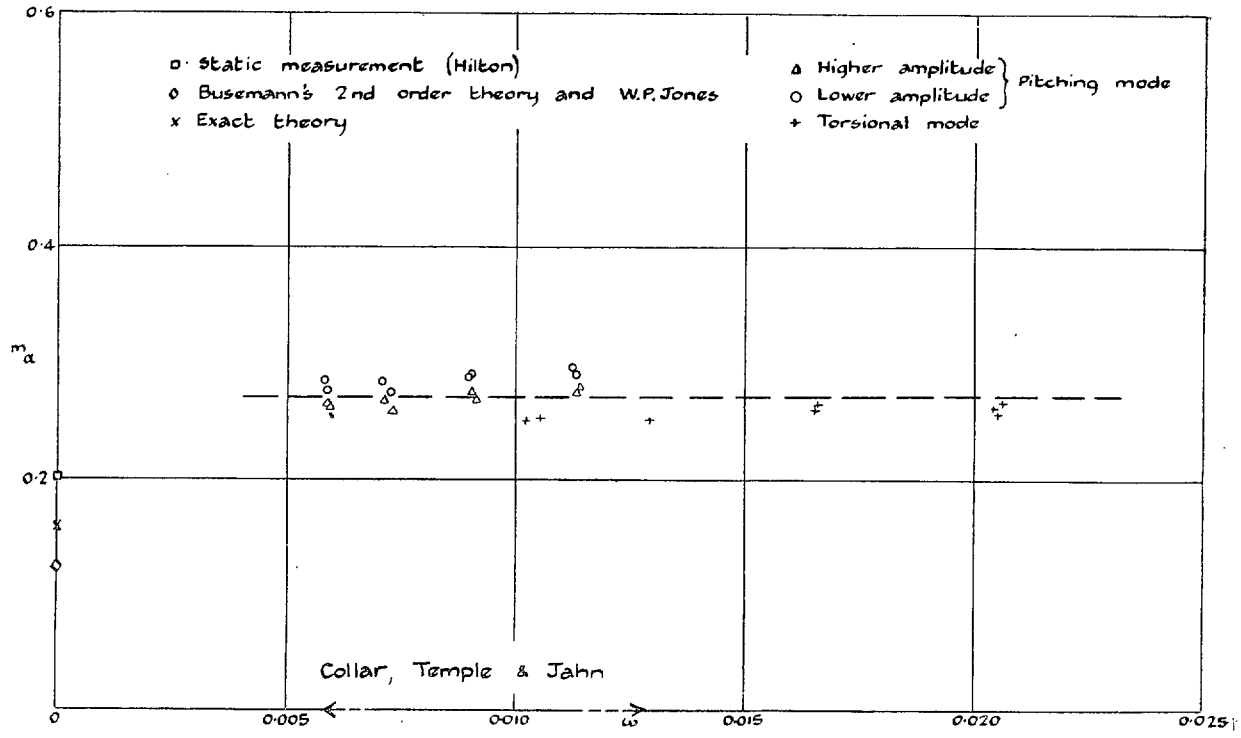

FIG. 15. Dependence of m_α on ω for $M = 1{\cdot}455$ (mean value).

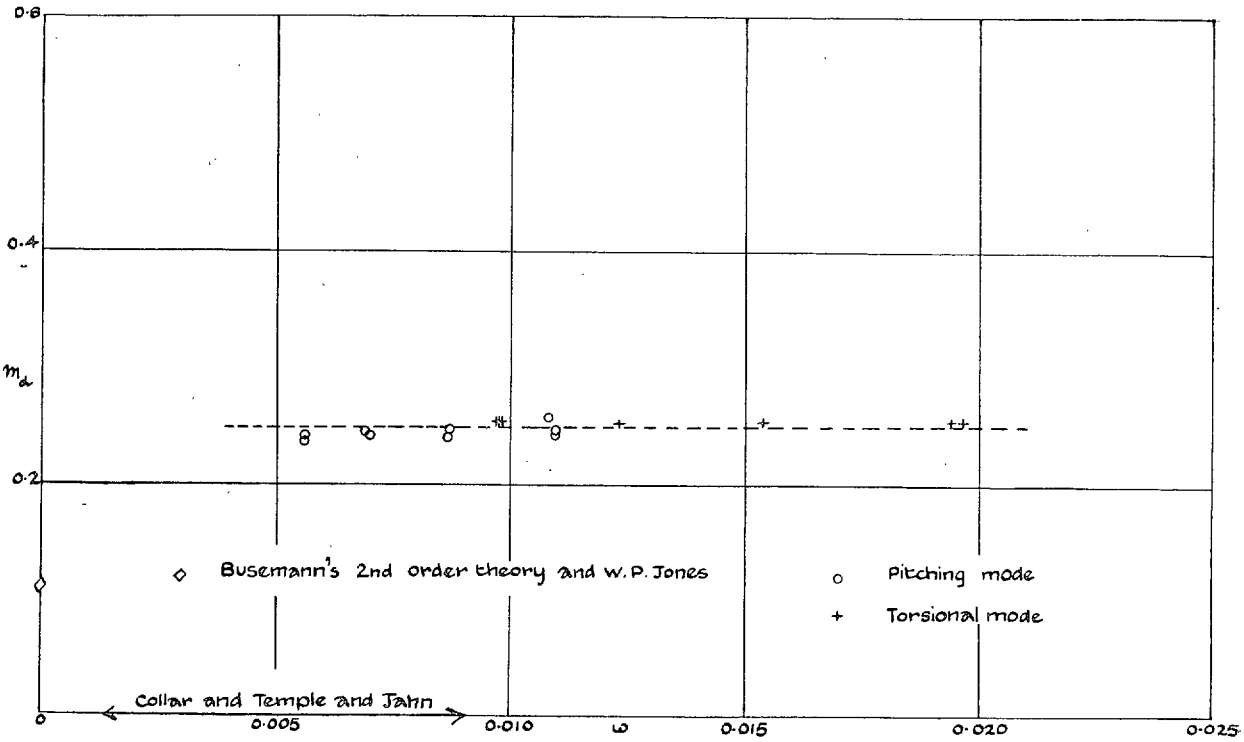

FIG. 16. Dependence of m_α on ω for $M = 1{\cdot}515$ (mean value).

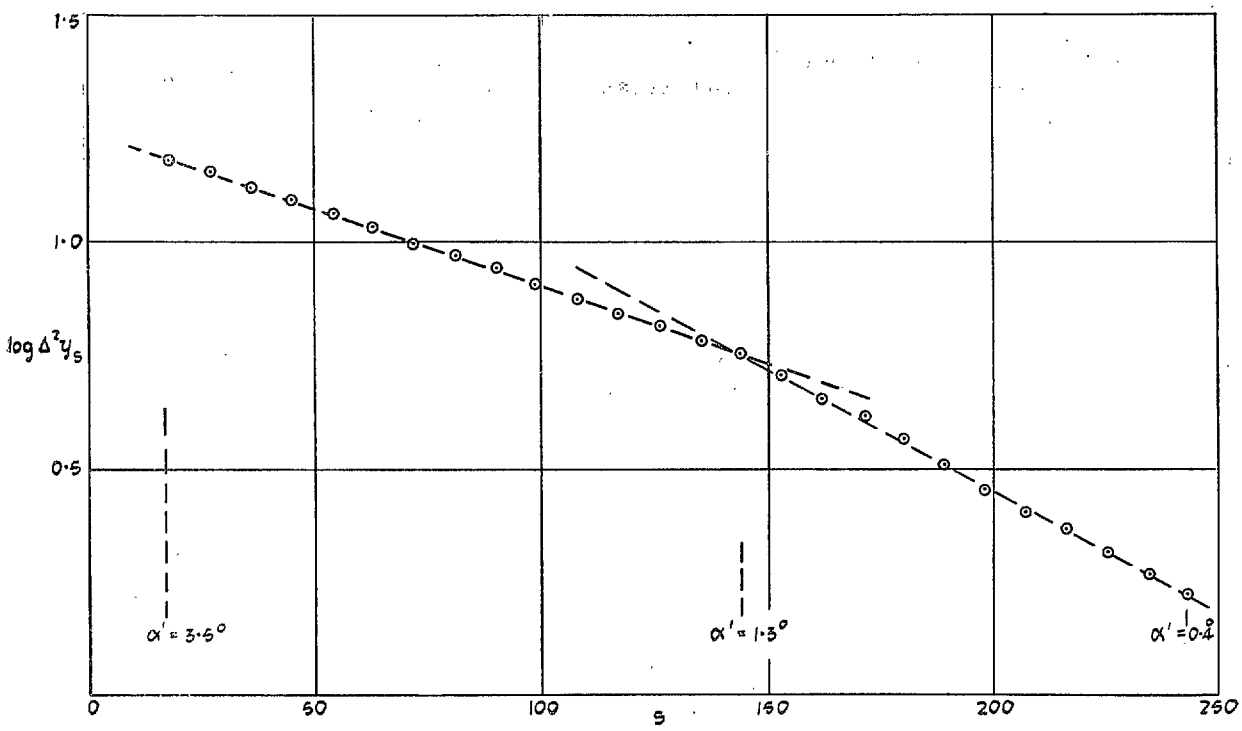

FIG. 17. Logarithmic decrement curve for $M = 1 \cdot 275$ (pitching oscillation).

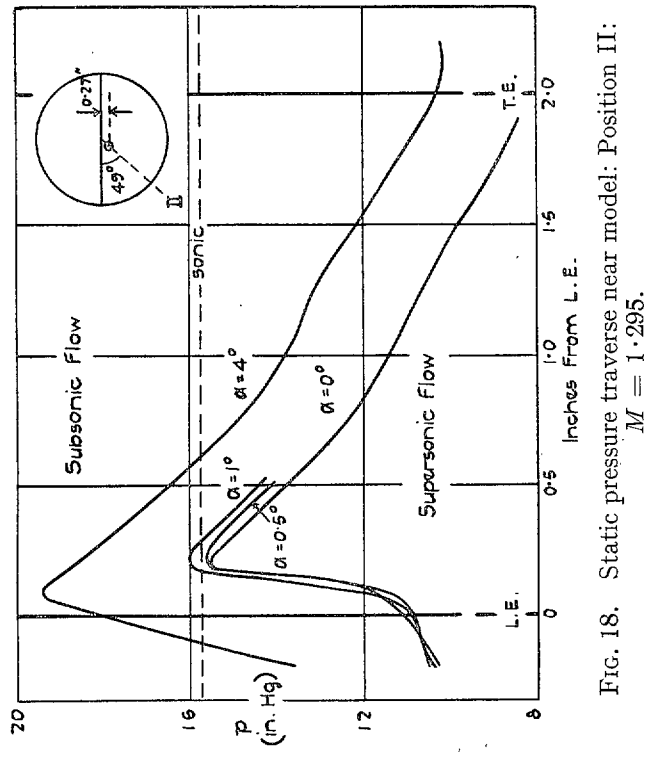

FIG. 18. Static pressure traverse near model: Position II: $M = 1 \cdot 295$.

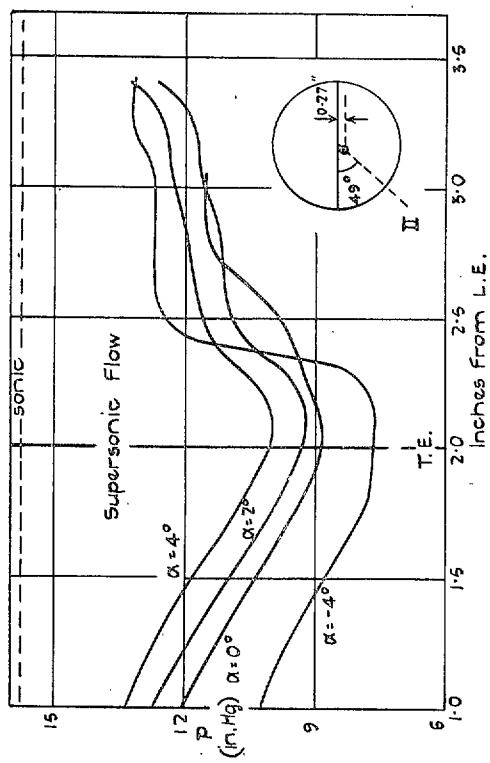

FIG. 19. Static pressure traverse near model: Position II: $M = 1 \cdot 300$.

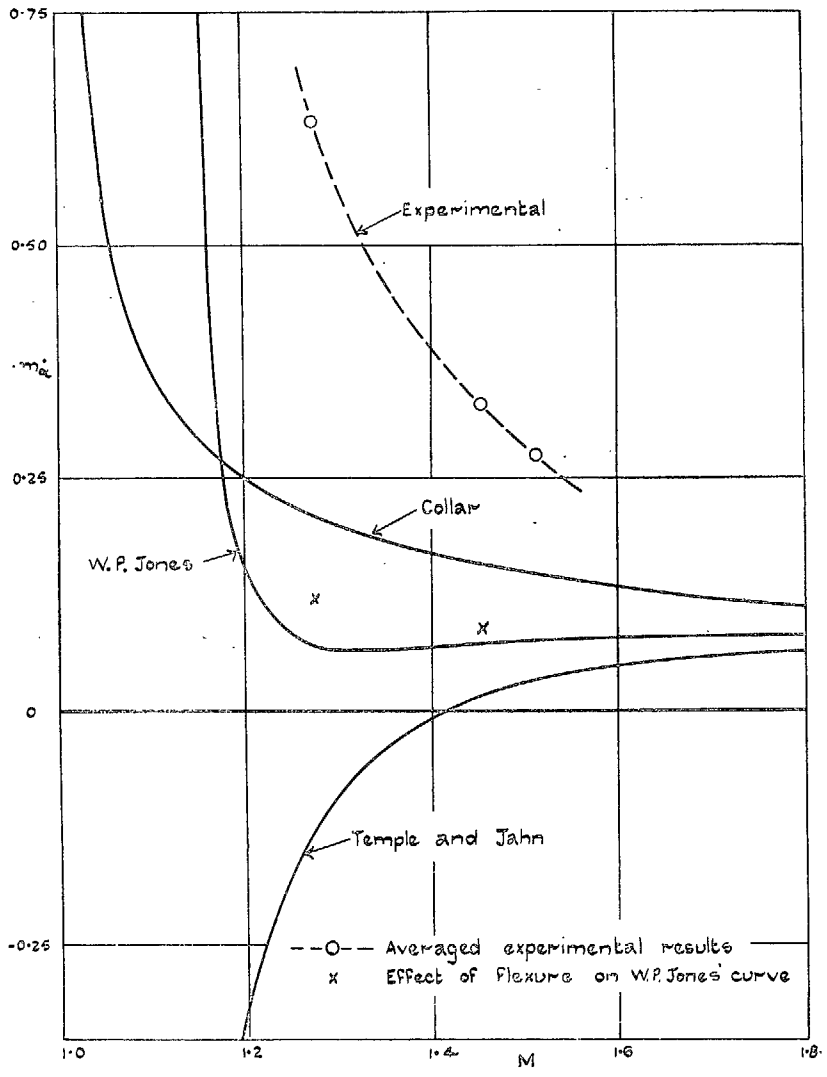

FIG. 20. Comparison of theoretical and experimental values of $m_{\dot{\alpha}}$ for supersonic flow ($\omega \to 0$).

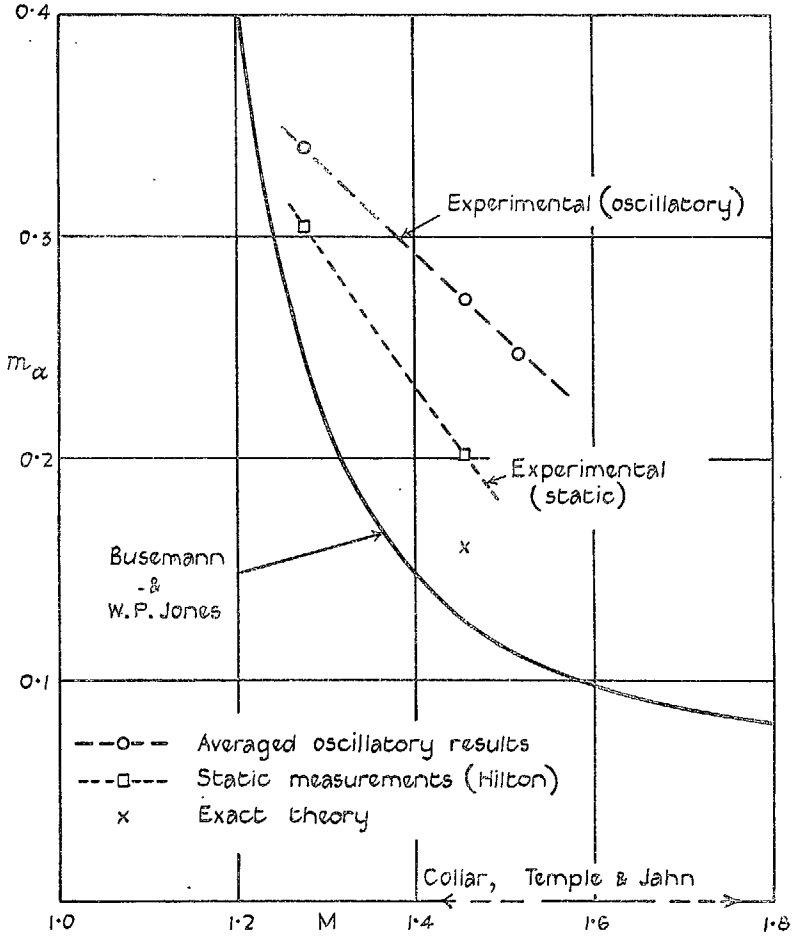

FIG. 21. Comparison of theoretical and experimental values of m_α for supersonic flow ($\omega \to 0$).

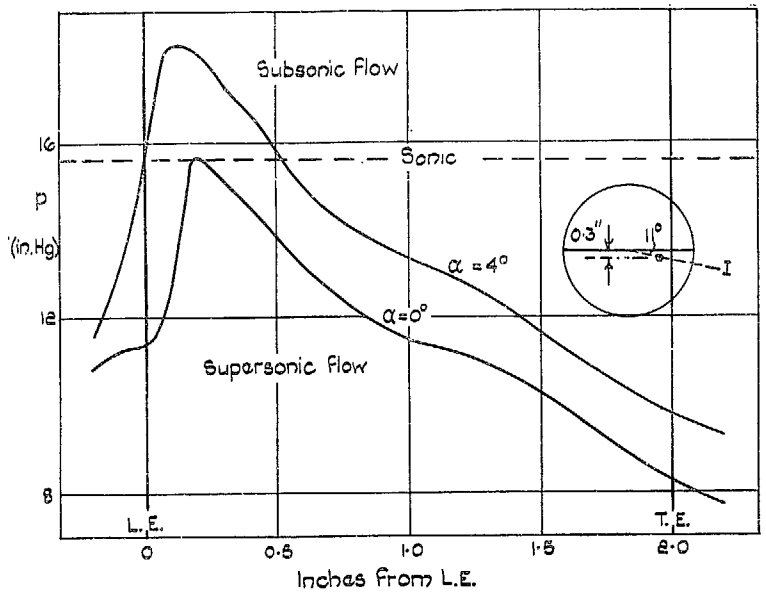

FIG. 22. Static pressure traverse near model: Position I: $M = 1 \cdot 300$.

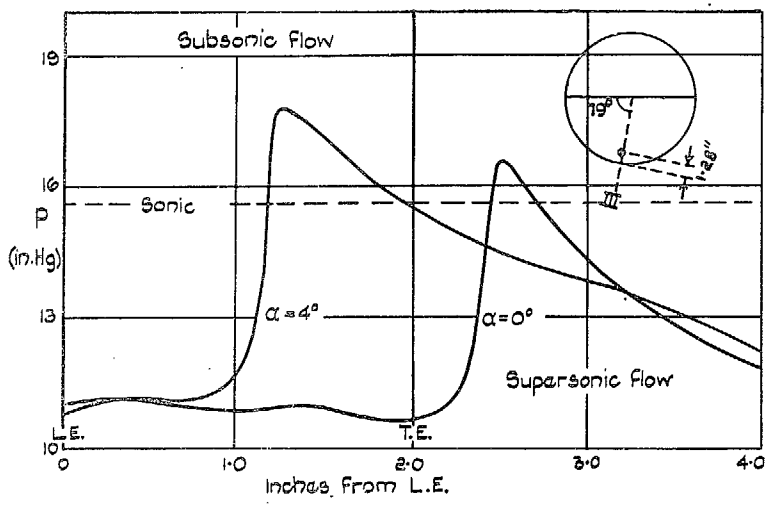

FIG. 23. Static pressure traverse near tunnel wall: Position III: $M = 1 \cdot 311$.

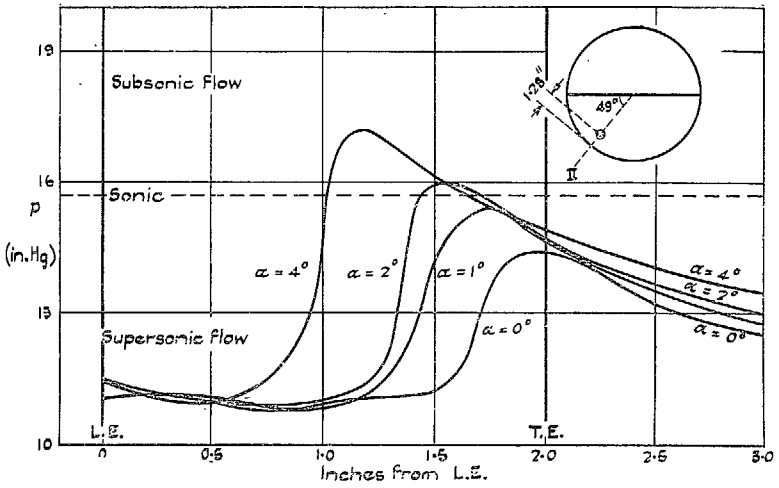

FIG. 24. Static pressure traverse near tunnel wall: Position II: $M = 1 \cdot 300$.

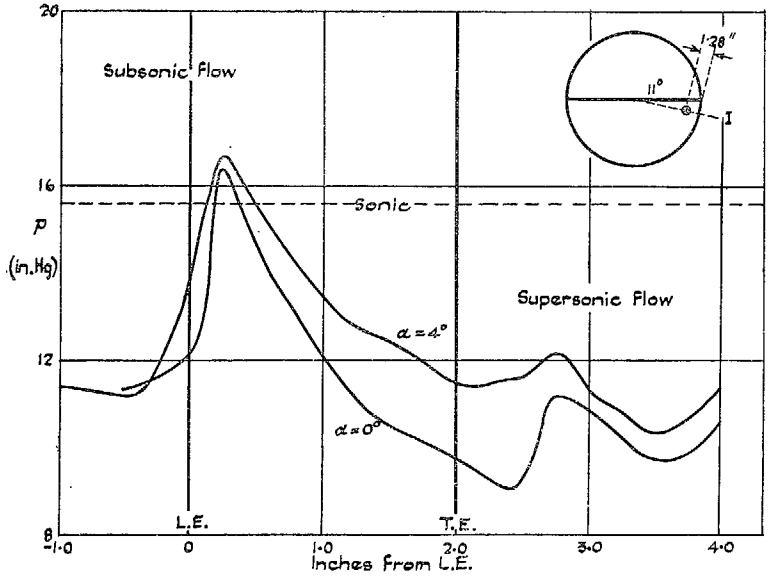

FIG. 25. Static pressure traverse near tunnel wall: Position I: $M = 1 \cdot 280$.

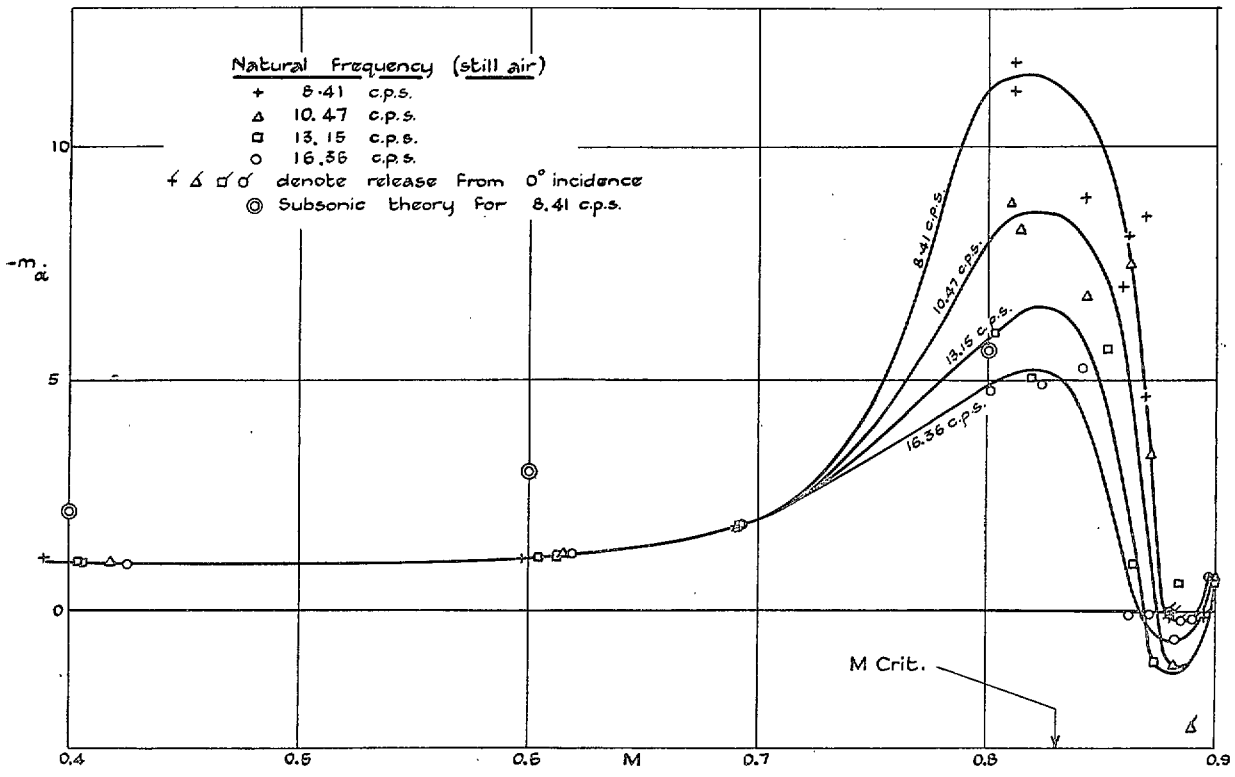

FIG. 26. Variation of $-m_{\dot{\alpha}}$ with M for subsonic speeds.

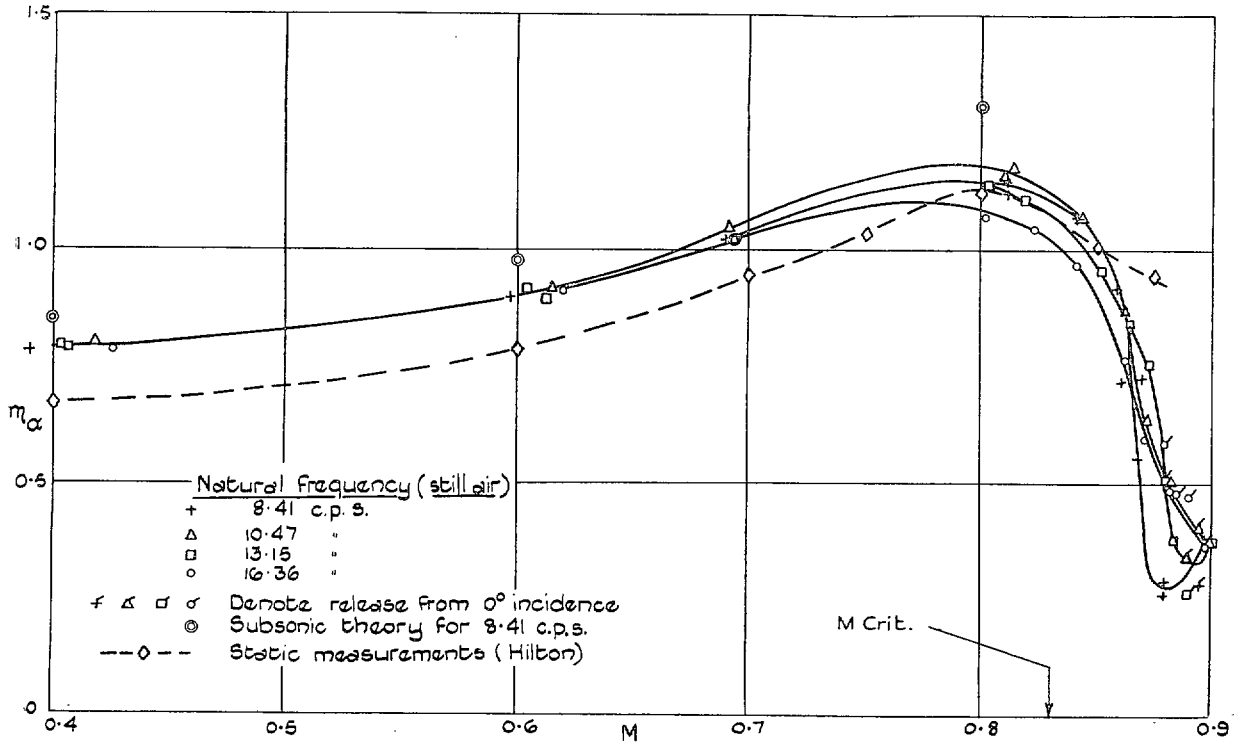

FIG. 27. Variation of m_α with M for subsonic speeds.

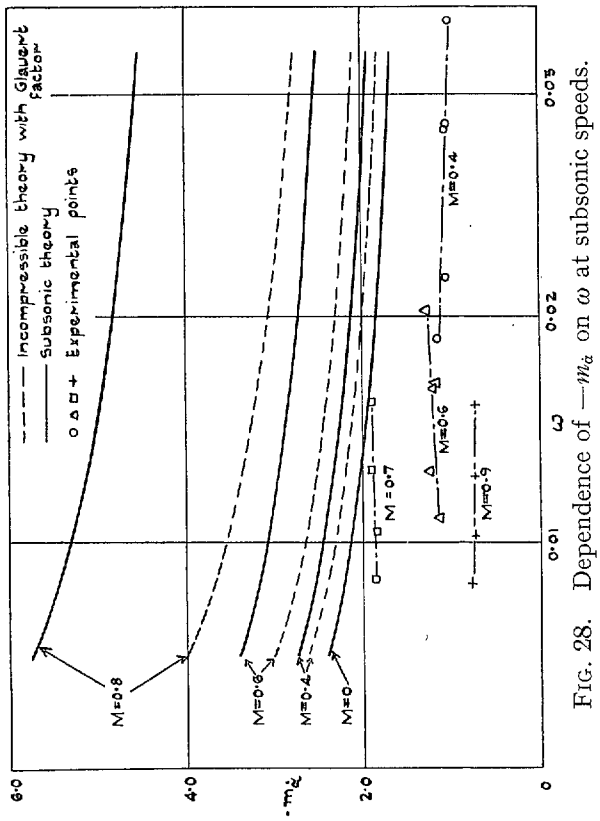

FIG. 28. Dependence of $-m_{\dot{\alpha}}$ on ω at subsonic speeds.

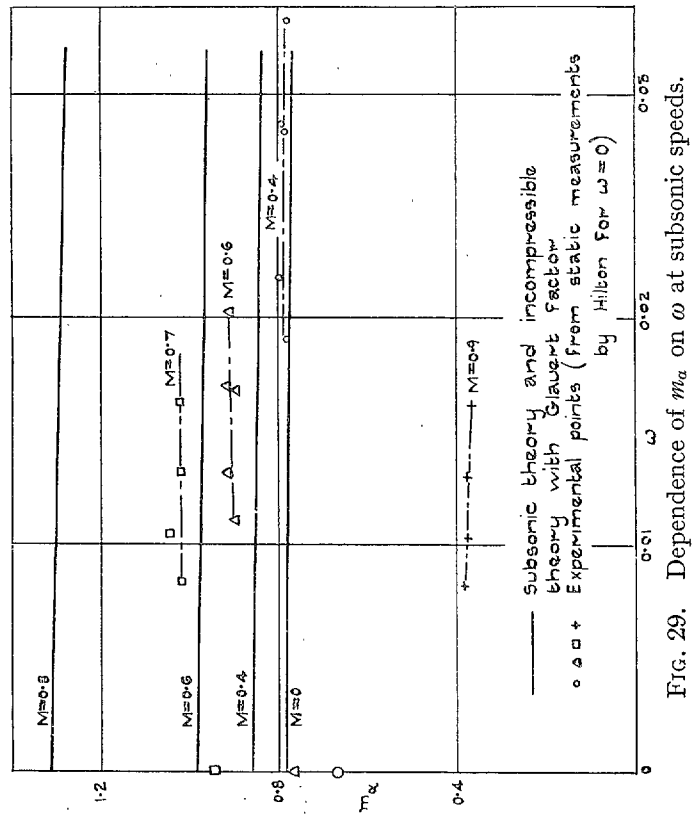

FIG. 29. Dependence of m_{α} on ω at subsonic speeds.

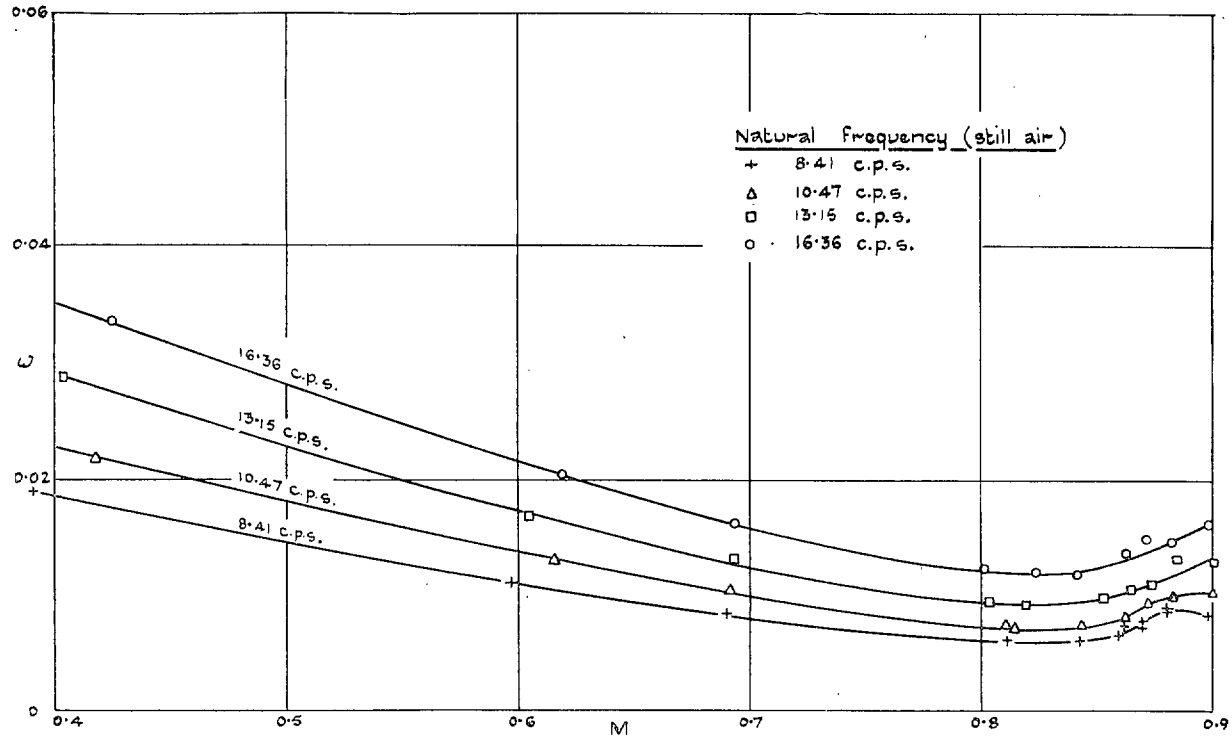

FIG. 30. Variation of ω with M in subsonic speed tests.

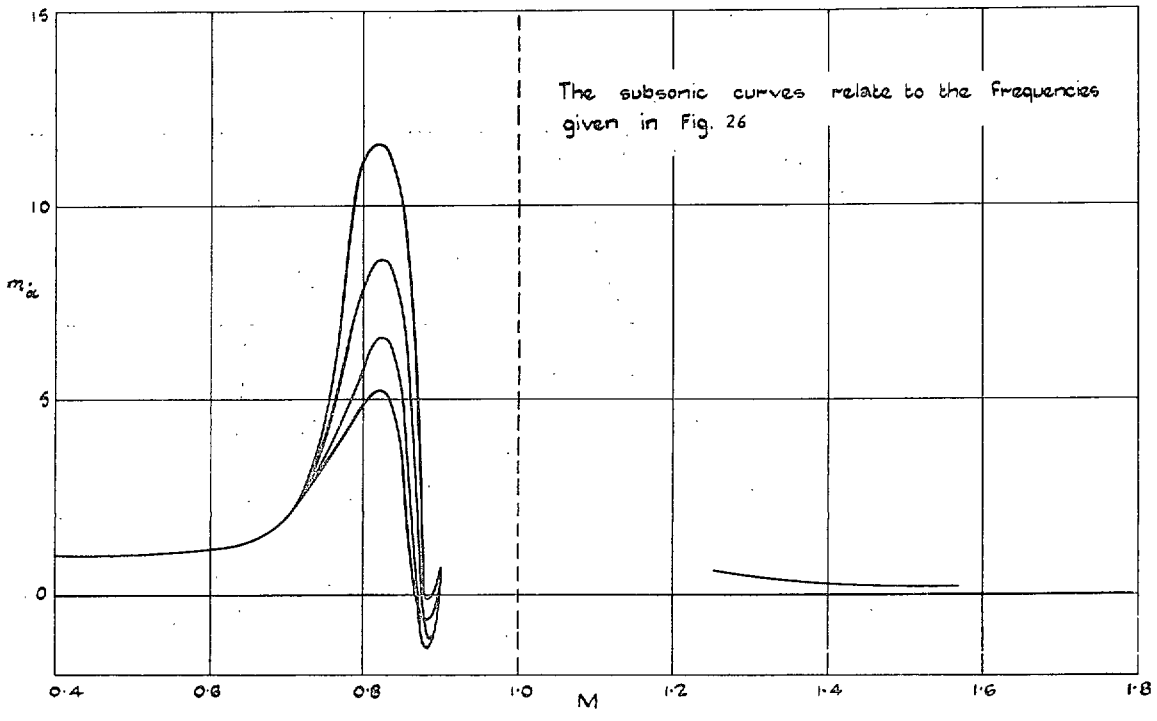

FIG. 31. Experimental values of $m_{\dot{\alpha}}$ for subsonic and supersonic speeds.

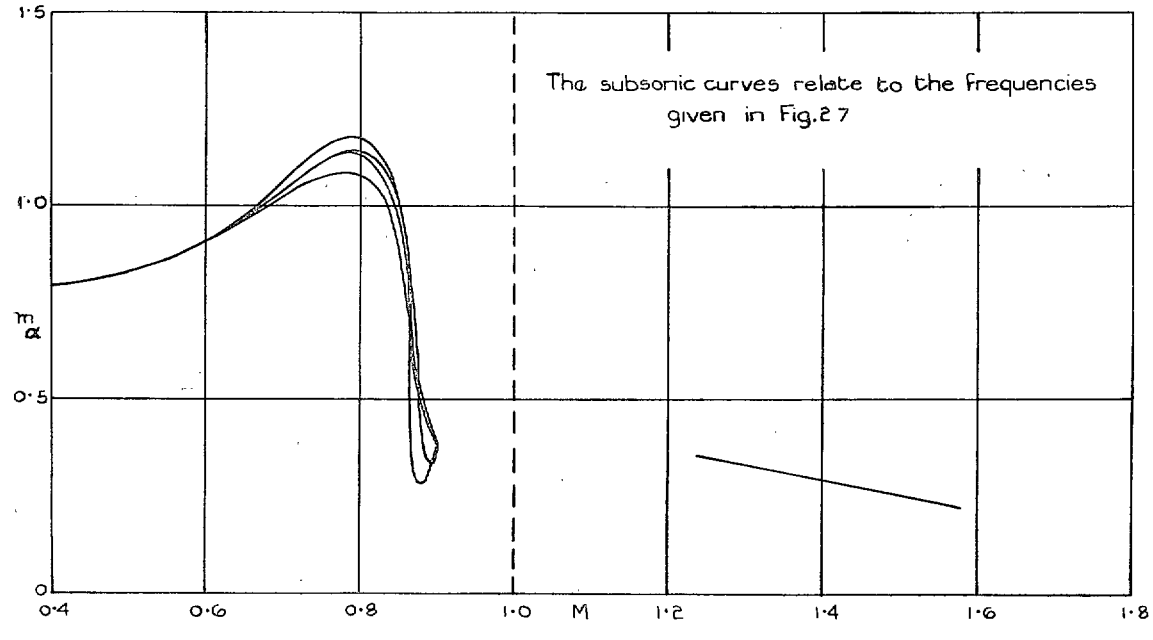

FIG. 32. Experimental values of m_{α} for subsonic and supersonic speeds.

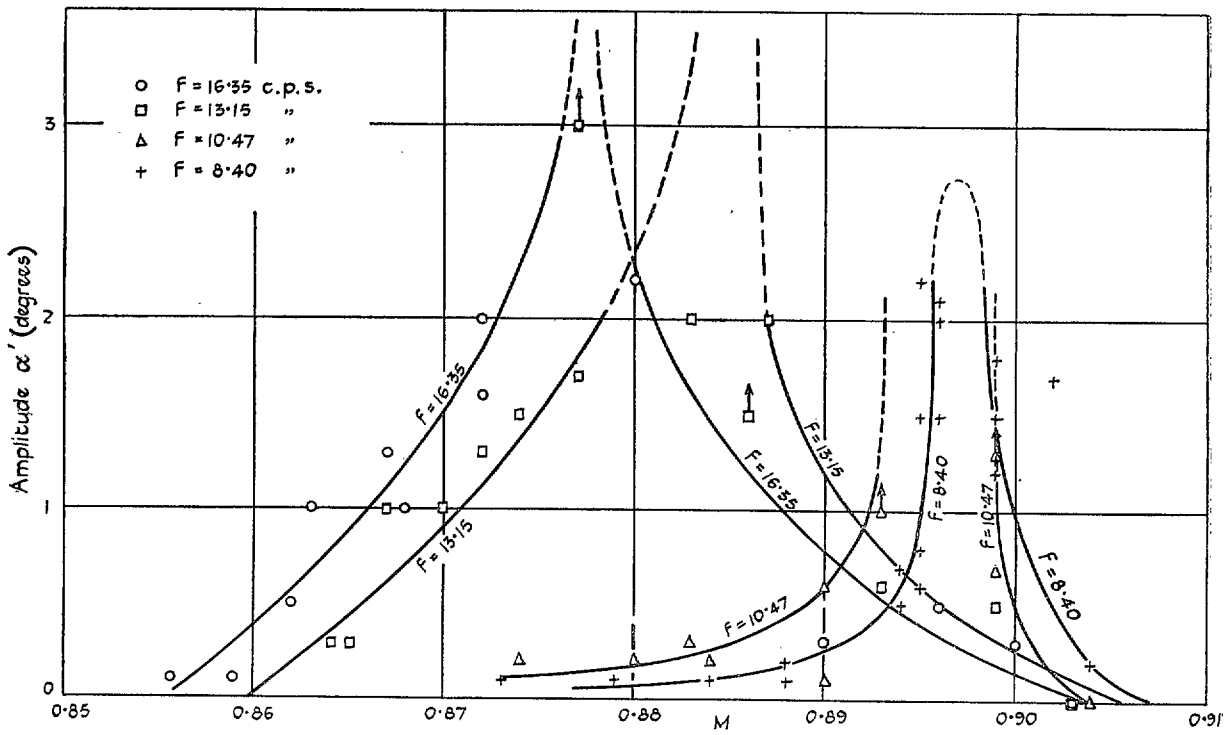

FIG. 33. Sustained pitching oscillations at subsonic speeds.

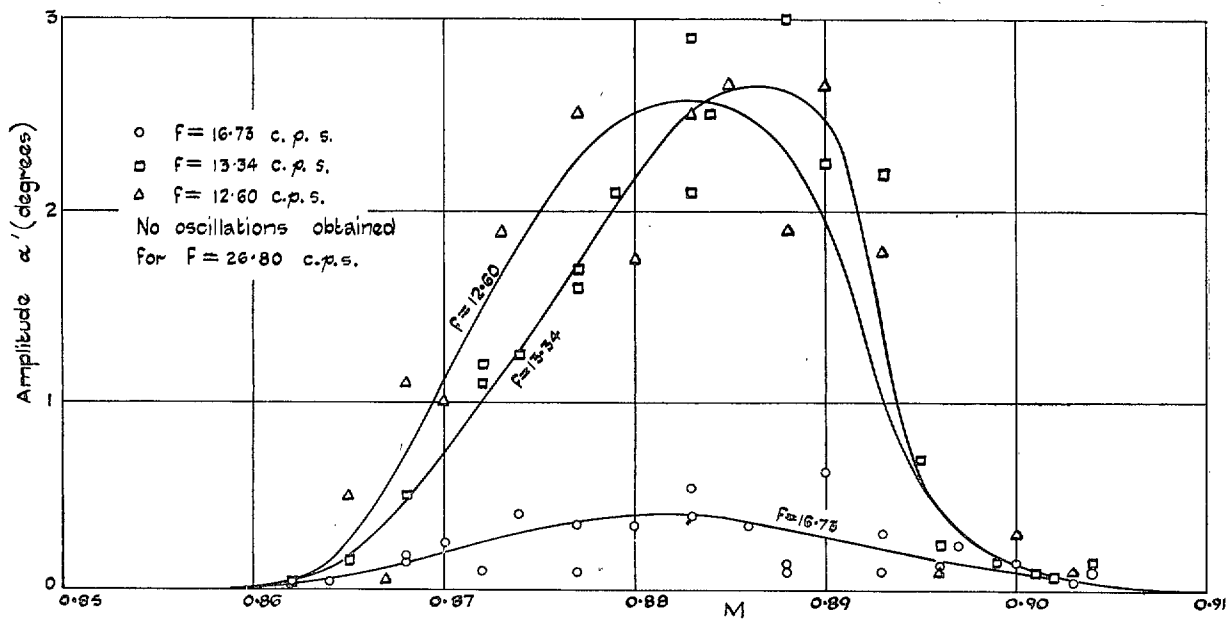

FIG. 34. Sustained torsional oscillations at subsonic speeds.

(932) Wt. 13/806 K.9 4/54 H.P.Co. 34-261

PRINTED IN GREAT BRITAIN

Publications of the Aeronautical Research Council

ANNUAL TECHNICAL REPORTS OF THE AERONAUTICAL RESEARCH COUNCIL (BOUND VOLUMES)—

1936 Vol. I. Aerodynamics General, Performance, Airscrews, Flutter and Spinning. 40*s.* (40*s.* 9*d.*)

Vol. II. Stability and Control, Structures, Seaplanes, Engines, etc. 50*s.* (50*s.* 10*d.*)

1937 Vol. I. Aerodynamics General, Performance, Airscrews, Flutter and Spinning. 40*s.* (40*s.* 10*d.*)

Vol. II. Stability and Control, Structures, Seaplanes, Engines, etc. 60*s.* (61*s.*)

1938 Vol. I. Aerodynamics General, Performance, Airscrews. 50*s.* (51*s.*)

Vol. II. Stability and Control, Flutter, Structures, Seaplanes, Wind Tunnels, Materials. 30*s.* (30*s.* 9*d.*)

1939 Vol. I. Aerodynamics General, Performance, Airscrews, Engines. 50*s.* (50*s.* 11*d.*)

Vol. II. Stability and Control, Flutter and Vibration, Instruments, Structures, Seaplanes, etc. 63*s.* (64*s.* 2*d.*)

* 1940 Aero and Hydrodynamics, Aerofoils, Airscrews, Engines, Flutter, Icing, Stability and Control, Structures, and a miscellaneous section. 50*s.* (51*s.*)

* 1941 Aero and Hydrodynamics, Aerofoils, Airscrews, Engines, Flutter, Stability and Control, Structures. 63*s.* (64*s.* 2*d.*)

* 1942 Vol. I. Aero and Hydrodynamics, Aerofoils, Airscrews, Engines. 75*s.* (76*s.* 3*d.*)

Vol. II. Noise, Parachutes, Stability and Control, Structures, Vibration, Wind Tunnels. 47*s.* 6*d.* (48*s.* 5*d.*)

* 1943 Vol. I. (*In the press*).

Vol. II. (*In the press*).

* *Certain other reports proper to these volumes will subsequently be included in a separate volume.*

ANNUAL REPORTS OF THE AERONAUTICAL RESEARCH COUNCIL—

1933–34	1*s.* 6*d.* (1*s.* 8*d.*)	1937	2*s.* (2*s.* 2*d.*)
1934–35	1*s.* 6*d.* (1*s.* 8*d.*)	1938	1*s.* 6*d.* (1*s.* 8*d.*)
April, 1935 to Dec. 31, 1936.	4*s.* (4*s.* 4*d.*)	1939–48	3*s.* (3*s.* 2*d.*)

INDEX TO ALL REPORTS AND MEMORANDA PUBLISHED IN THE ANNUAL TECHNICAL REPORTS, AND SEPARATELY—

April, 1950 . . . . . R. & M. No. 2600. 2*s.* 6*d.* (2*s.* 7½*d.*)

AUTHOR INDEX TO ALL REPORTS AND MEMORANDA OF THE AERONAUTICAL RESEARCH COUNCIL—

1909–1949 . . . . . R. & M. No. 2570. 15*s.* (15*s.* 3*d.*)

INDEXES TO THE TECHNICAL REPORTS OF THE AERONAUTICAL RESEARCH COUNCIL—

December 1, 1936 — June 30, 1939.	R. & M. No. 1850.	1*s.* 3*d.* (1*s.* 4½*d.*)
July 1, 1939 — June 30, 1945.	R. & M. No. 1950.	1*s.* (1*s.* 1½*d.*)
July 1, 1945 — June 30, 1946.	R. & M. No. 2050.	1*s.* (1*s.* 1½*d.*)
July 1, 1946 — December 31, 1946.	R. & M. No. 2150.	1*s.* 3*d.* (1*s.* 4½*d.*)
January 1, 1947 — June 30, 1947.	R. & M. No. 2250.	1*s.* 3*d.* (1*s.* 4½*d.*)
July, 1951.	R. & M. No. 2350.	1*s.* 9*d.* (1*s.* 10½*d.*)

Prices in brackets include postage.

Obtainable from

HER MAJESTY'S STATIONERY OFFICE

York House, Kingsway, London, W.C.2; 423 Oxford Street, London, W.1. (Post Orders; P.O. Box 569, London, S.E.1); 13a Castle Street, Edinburgh 2; 39 King Street, Manchester 2; 2 Edmund Street, Birmingham 3; 1 St. Andrew's Crescent, Cardiff; Tower Lane, Bristol 1; 80 Chichester Street, Belfast OR THROUGH ANY BOOKSELLER.

S.O. Code No. 23-2680